THREE-DIMENSIONAL ACOUSTIC IMPEDANCE MAP ANALYSIS OF SOFT TISSUE

BY

ALEXANDER J. DAPORE

THESIS

Submitted in partial fulfillment of the requirements
for the degree of Master of Science in Electrical and Computer Engineering
in the Graduate College of the
University of Illinois at Urbana-Champaign, 2010

Urbana, Illinois

Advisers:

Professor William D. O'Brien, Jr.
Associate Professor Minh N. Do

Abstract

Three-dimensional impedance maps (3DZMs) are virtual volumes of acoustic impedance values constructed from histology to represent tissue microstructure acoustically. From the 3DZM, the ultrasonic backscattered power spectrum can be predicted and model based scatterer properties, such as effective scatterer diameter (ESD), can be estimated. Additionally, the 3DZM can be exploited to visualize and identify possible scattering sites, which may aid in the development of more effective scattering models to better represent the ultrasonic interaction with underlying tissue microstructure.

The 3DZM construction and analysis algorithms have been improved both in terms of performance and cost. A multiresolution registration scheme has been implemented in order to robustly reconstruct the 3DZM from real tissue. Additional processing, such as photometric correction and automatic detection of damaged histology sections, has been applied to ensure the reconstructed volume is faithful to the properties of the orignal tissue.

In this work, 3DZMs were created from a set of human fibroadenoma samples. ESD estimates were made assuming a fluid-filled sphere form factor model from 3DZMs of volume 300x300x300 μm^3. For a collection of 33 independent human fibroadenoma tissue samples, the ESD was estimated to be 111.4$\pm$40.7 μm. The 3DZMs were then investigated visually to identify possible scattering sources which conformed to the estimated model scatterer dimensions.

Additionally, 3DZMs were compared with quantitative ultrasound (QUS) techniques. A

chemically fixed section of rabbit liver was scanned ultrasonically, then used to create 3DZMs. ESD estimates were made using the fluid-filled sphere form factor. Twenty-four 3DZMs of volume 300x300x300 μm^3 were constructed from the sample, and using two methods of ESD estimation, produced ESD estimates of 93.6$\pm$52.7 and 7.04$\pm$1.30 μm. ESD was also estimated from ultrasonic backscatter using transducers with center frequencies 7.5, 13, 20, 40, and 65 MHz. The ESD estimates from the backscatter data were 102.2$\pm$30.5, 63.3$\pm$12.2, 23.6$\pm$26.2, 19.8$\pm$1.1, and 2.78$\pm$6.43 μm respectively.

This work provides new insights into the 3DZM technique, both in terms of its viability for tissue studies and its relationship to more traditional QUS techniques.

Acknowledgments

This work would not have been possible without the important contributions of many individuals. First, I would like to thank my advisers Dr. Minh N. Do and Dr. William D. O'Brien, Jr., whose guidance has led not only to the development of this project, but to my own advancement as an engineer, researcher, and person. I must also thank the Bioacoustics Research Lab, specifically the contributions of Dr. Michael L. Oelze, Dr. Lauren A. Wirtzfeld, and Dr. Rita J. Miller. And finally, I recognize the continual support and guidance of my parents, Mark and Michelle; my brother, Corey; and my sister, Marissa.

This work was funded by NIH Grant CA111289.

Contents

Chapter 1

Introduction

Medical ultrasound provides a safe, portable, and inexpensive imaging modality when compared to other common modalities such as X-ray, computed tomography, or magnetic resonance imaging [1, 2]. These advantages clearly motivate the development of additional diagnostic functionality in medical ultrasound. While conventional ultrasound images provide mainly qualitative depictions of tissue macrostructure, quantitative ultrasound (QUS) provides quantitative information about tissue microstructure. This information could greatly improve the diagnostic functionality in medical ultrasound. This process, however, depends on the use of appropriate models for ultrasonic scattering by tissue microstructure [3].

As a means to investigate such ultrasonic scattering, a method was previously developed to create computational acoustic models of tissue microstructure [1]. These models, called three-dimensional impedance maps (3DZMs), provide a means to combine ultrasonic characterization of tissue with histological evaluation of the underlying tissue structure. This study investigates the application of these models to a common type of benign human breast tumor, the fibroadenoma.

1.1 Quantitative Ultrasound

Conventional ultrasound images are derived from backscattered radio frequency (RF) echo signals, which are a result of scattering by tissue macro- and microstructure with varying acoustic properties. Typically, the received RF signals are envelope detected to produce an image; this processing removes frequency-dependent information from the RF signal [4].

Some QUS techniques use the frequency-dependent information from the RF echo signal to deduce quantitative information related to the properties of the tissue microstructure. This frequency-dependent information can provide details about statistical properties of scattering structures, such as effective scatterer diameter (ESD) and effective acoustic concentration. Parameterization of ultrasonic backscatter has been investigated previously as a means to extend the diagnostic capability of ultrasound [5, 6], and has demonstrated the ability to quantify ocular, liver, prostate, renal, and cardiac tissues [7]. To attain more meaningful results, however, the relationship between backscattered frequency-dependent information and underlying tissue properties must be better understood.

1.2 Three-Dimensional Impedance Maps

A 3DZM is an acoustic, computational model of tissue, and a tool to aid in the understanding of small scale acoustic scattering. Currently, 3DZMs are volumes constructed from properly aligned and reconstructed sets of histological images. The value of each volume element (voxel) of the 3DZM represents an acoustic impedance value.

For weakly scattering media (the acoustic impedance of scattering objects is very close to the acoustic impedance of the background material), the autocorrelation function of the spatial impedance map can be related to the ultrasonic backscatter of the media by the spatial Fourier transform [1]. In this way, 3DZMs can be used to study both the ultrasonic backscatter and the histological characteristics of a particular medium. This duality

illustrates the utility of 3DZMs for the study of ultrasonic scattering in tissue as it relates ultrasonic backscatter to actual histological features of tissue microstructure.

This study expands upon the 3DZM work previously done by Mamou et al. [1]. The 3DZM creation process has been updated, giving improvements in both performance and computational efficiency. Additionally, this work is the first time a large number of tissue samples have been analyzed via 3DZM. Using 3DZMs, 33 human fibroadenomas were analyzed, giving insight into both the 3DZM technique as well as quantitatively characterizing these benign tumors. This work also attempts to begin to quantify the link between 3DZM based techniques and ultrasonic backscatter techniques. A chemically fixed sample of rabbit liver was examined using both modalities, and the ESD estimation process was compared.

Chapter 2

Acoustic Theory

2.1 Quantitative Ultrasound

Ultrasonic scattering occurs when an incident pressure wave interacts with a volume having spatially varying acoustic properties. Ultrasonic backscatter is defined as the portion of this scattered sound that propagates in the opposite direction of the incident wave, which is of special interest for pulse-echo ultrasound [2].

For a plane wave of unit amplitude, the far field backscattered pressure from a scattering volume can be described by

$$p_b(r,k) = \frac{e^{-jkr}}{r}\Phi(2k), \tag{2.1}$$

where r is the distance to the scattering site, k is the spatial frequency or acoustic wave number (defined as the ratio of the angular frequency of the acoustic wave to the speed of sound in the medium), and $\Phi(2k)$ is an angle distribution function [6]. The acoustic intensity for the backscattered wave in (2.1) can be expressed by

$$I_b = A|\Phi(2k)|^2, \tag{2.2}$$

where A is a proportionality constant [2]. Through methods described in [1, 6], the backscattered intensity can be computed as a function of frequency, and related to the acoustic impedance of the underlying tissue. By making the assumption of weak scattering, which is appropriate in soft tissue, (2.2) can be rewritten as

$$I_b = A' k^4 S(2k), \tag{2.3}$$

where A' is a new proportionality constant, and $S(2k)$ is the squared magnitude of the Fourier transform of a relative impedance function [8]. The equation describing $S(2k)$ is

$$S(2k) = \left| \iiint_V \frac{z(r) - z_0}{z_0} e^{-2jkr} dV \right|^2, \tag{2.4}$$

where z_0 is the acoustic impedance of the background material and $z(r)$ is the spatially varying acoustic impedance at position r. The background impedance is defined as

$$z_0 = \sqrt{\frac{\rho_0}{\kappa_0}}, \tag{2.5}$$

where ρ_0 is the density and κ_0 is the compressibility of the background material. Likewise, the scatterer impedance is defined as

$$z(r) = \sqrt{\frac{\rho(r)}{\kappa(r)}}, \tag{2.6}$$

where $\rho(r)$ is the spatially varying density and $\kappa(r)$ is the spatially varying compressibility at position r.

2.2 Intensity Form Factor

Intensity form factors (FFs) are functions that describe the behavior of the backscattered intensity due to a single scattering volume as a function of k [9]. Form factors model the deviation in the frequency dependence of the backscatter coefficient for a particular scattering volume from the frequency dependence observed for a Rayleigh scatterer (which has only a k^4 dependence). The development of the intensity form factor in [10] considers identical fluid spheres of diameter d randomly distributed in a homogeneous background. If a scattering volume has spherical symmetry, then the corresponding FF function will only depend on the scatterer size, because the orientation of the volume is not important. In this case, scatterer size refers to either the effective diameter for discrete scatterers or to the effective correlation length for scatterers that are continuously varying functions [9]. In this situation, a fluid-filled sphere, the backscatter coefficient is given as

$$\sigma_b = \frac{k^4 V_s^2 \bar{n} \gamma_0^2}{16\pi^2} \left(\frac{3}{kd} j_1(kd) \right)^2, \tag{2.7}$$

where V_s is the effective scatterer volume, $\bar{n}\gamma_0^2$ is the scattering strength, and j_1 is the first order spherical Bessel function of the first kind. In the long wavelength or Rayleigh limiting case, the backscatter coefficient is defined as

$$\sigma_0 = \frac{k^4 V_s^2 \bar{n} \gamma_0^2}{16\pi^2}. \tag{2.8}$$

The backscatter coefficient σ_b can be written as a function of σ_0,

$$\sigma_b = \sigma_0 F(2k, d), \tag{2.9}$$

where $F(2k, d)$ is the intensity form factor. By substituting (2.7) and (2.8) into (2.9), the FF for a fluid-filled sphere scatterer is given by

$$F(2k, d) = \left(\frac{3j_1(kd)}{kd} \right)^2. \tag{2.10}$$

Regardless of the scattering volume geometry, the corresponding FF always approaches unity as k approaches zero because as the wavelength becomes very large, the scatterer appears as a point scatterer. Figure 2.1 shows a plot of the fluid-filled sphere FF as a function of spatial frequency k for several values of d.

Form factors are related to the geometry of the scatterer by the Fourier transform of the 3D spatial autocorrelation function of the acoustic impedance distribution [10], or equivalently by the squared magnitude of the 3D spatial Fourier transform of the impedance distribution (due to the Wiener-Khintchine theorem) [8]. Because of this, FFs are proportional to the power spectrum $S(2k)$ of a scattering volume as described by (2.4). This motivates the use of 3DZMs in tissue acoustic analysis. By constructing the spatial distribution of the impedance for a tissue volume, the corresponding ultrasonic backscatter power spectrum can be estimated. The 3DZM method uses histology information from a given tissue sample to accurately reconstruct a spatially varying acoustic impedance distribution in the volume. By estimating the power spectrum from the data-specific 3DZM, FFs can be used as scattering models to extract diagnostically useful QUS model-based parameters, such as ESD.

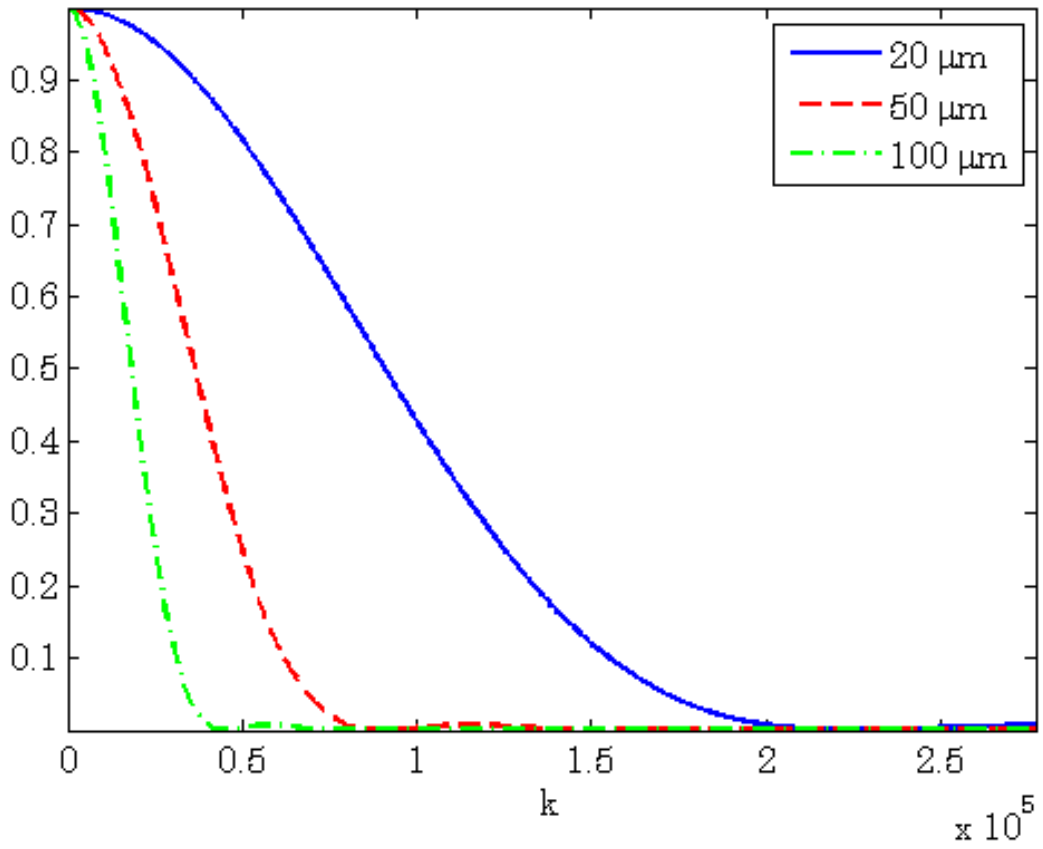

Figure 2.1: Fluid-filled sphere form factor for $d = 25, 50, 100$ μm.

Chapter 3

Impedance Map Construction

3.1 Construction Overview

A 3DZM is a computational phantom of which each element represents an estimate of the acoustic impedance value of the underlying medium at a particular location. A technique for the creation of 3DZMs was developed previously by Mamou et al. [1, 11]. In the current study, a novel 3DZM construction process has been developed that improves upon the previous method in terms of both performance and computational efficiency. A block diagram of the improved process is shown in Figure 3.1.

3.2 Histology Data Acquisition

The goal of 3DZM creation is to build a computational model that acoustically mimics real tissue. To accomplish this objective, each 3DZM is constructed from a tissue sample. To start the process, the sample is prepared for histology where it is fixed in formalin, embedded in paraffin, sectioned at a thickness of 3 μm, placed on glass slides, and stained with hematoxylin and eosin (H&E). Each section is individually digitized using a NanoZoomer HT slide scanner

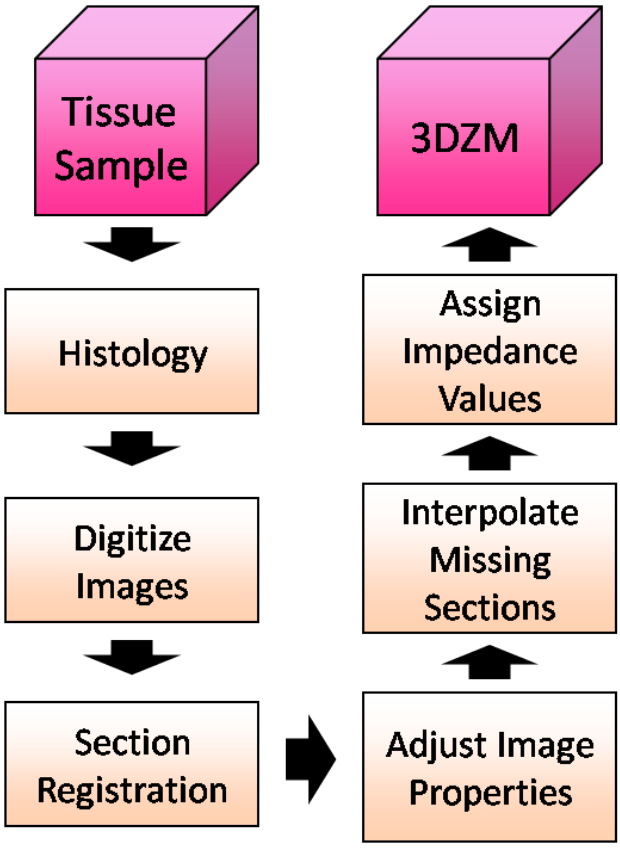

Figure 3.1: 3DZM creation process block diagram.

(Hamamatsu, Hamamatsu City, Japan) at a pixel resolution of 0.46 μm. The image is quantized in red, green, and blue color fields (RGB color), at 24 bits per pixel. Figure 3.2 shows a portion of one digitized fibroadenoma section.

3.3 Artifact Correction

In order for this set of 2D images to be converted into a 3D volume, artifacts inherent to the preparation process must be corrected. During the histology process, the individual sections undergo a certain degree of unintended shrinking and shearing, and are placed on glass slides in a variety of orientations. These 2D images need to be properly registered to

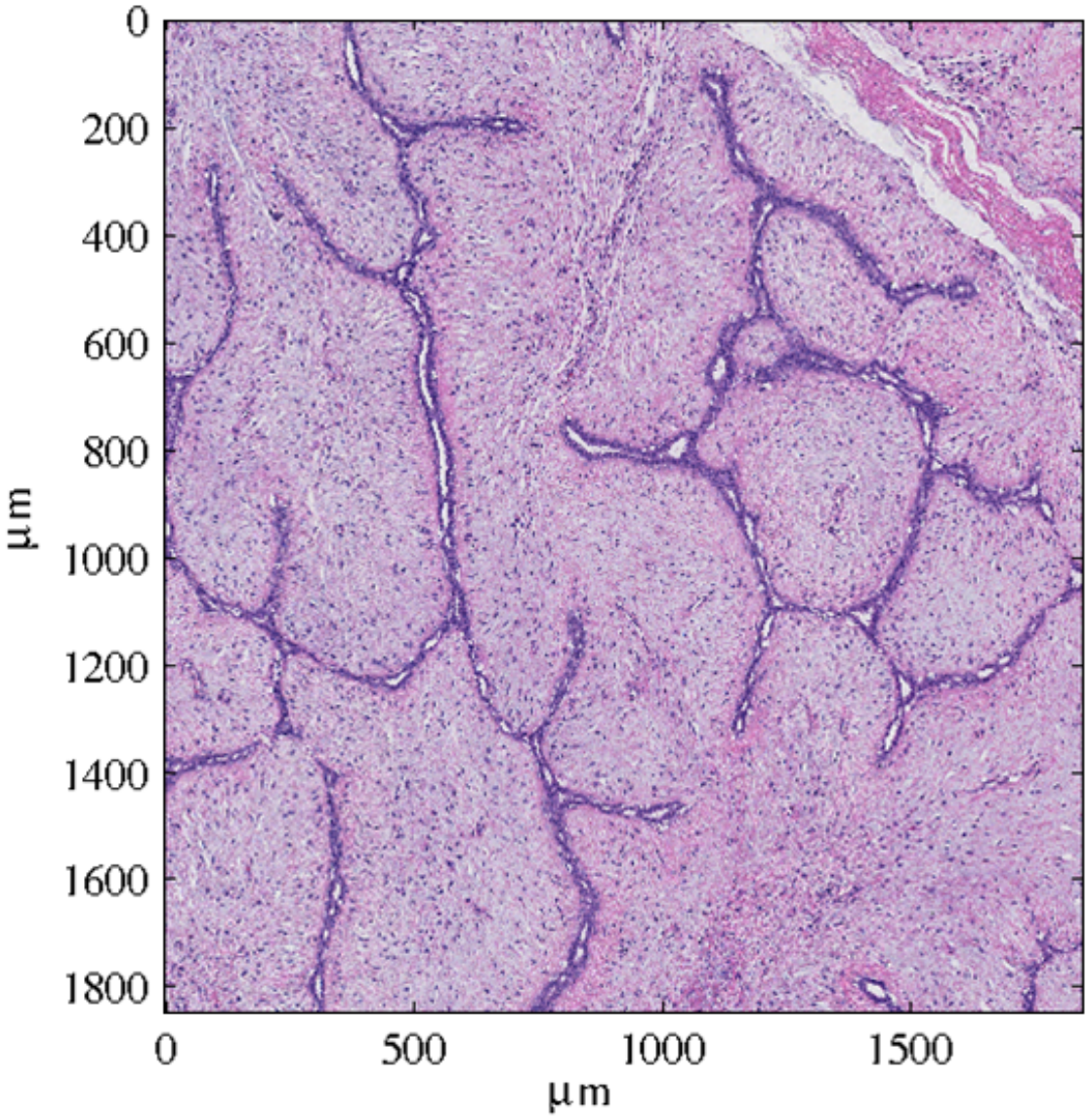

Figure 3.2: An H&E stained fibroadenoma 3 μm thick section that is 1800 μm x 1800 μm.

adjacent sections so that their position within the original 3D volume is properly restored. Due to the size of the individual images (in this study, the high resolution tissue images often reached 30,000 pixels on a side), and the fact that only a small portion of the total slice will be present inside a single 3DZM, the registration process is broken into two stages.

Each stage operates at a different resolution level. The first registration stage provides a very rough alignment at the global level. Performing registration at this level provides the benefit of being able to use the edges of the tissue sample to align adjacent sections. Each image is decimated until it has roughly 100 rows of pixels and has the same aspect ratio as the full size image. Rigid registration parameters (translation and rotation) are estimated using a correlation metric. For two adjacent images I and J, the correlation metric is given by

$$\text{corr}(I, J) = \frac{E[(I - \mu_I)(J - \mu_J)]}{\sigma_I \sigma_J}, \tag{3.1}$$

where μ is the mean and σ is the standard deviation of its respective image. The translation and rotation values that maximize (3.1) are chosen as the proper alignment values at this resolution, and are passed on as initial guesses for the finer resolution registration stages.

At the global registration stage, the quality of each histologic slice is automatically examined. Sections that have a substandard correlation metric with their neighboring sections are considered unusable and are removed from any further processing steps. A poor correlation score is typically indicitive of tearing, folding, or another irreversible artifact caused during the histology process. It is important to remove these damaged sections, as these sections will often generate erroneous registration parameters when a good alignment is not possible. When the volume is reconstructed, these errors will cascade and cause significant discontinuities in the histology volume. Any sections removed during this stage are interpolated at a later stage, and the neighboring sections are aligned to each other in order to preserve continuity.

For the local, fine resolution registration stage, the deformation model is altered to allow for more complex geometric misalignments. In addition to simple translational and rotational (rigid) registration, the sections must be adjusted for any stretching or shearing that occurred as a result of the tissue slicing, staining process, or placement onto each glass slide. An

affine model is used to describe the geometric deformations to be corrected, and is given for a warped image I' and the true image I by

$$I'(\mathbf{x}) = \mathbf{I}(\mathbf{A}\mathbf{x} + \mathbf{b}), \tag{3.2}$$

$$\mathbf{A} = \begin{bmatrix} a_{11} & a_{12} \\ a_{21} & a_{22} \end{bmatrix}, \mathbf{b} = \begin{bmatrix} b_1 \\ b_2 \end{bmatrix}, \tag{3.3}$$

where the matrix $\mathbf{A}$ describes stretching, shearing, and rotational components, and the vector $\mathbf{b}$ describes translational components of the geometric misalignments. Before the full affine parameter set is optimized, the initial conditions are perturbed through a set of random trials. The translation and rotation parameters are summed with independent uniform random variables ranging from -40 to 40 pixels and -10 to 10 degrees respectively. After 200 such trials, the set of parameters that result in the best mutual information metric are chosen as initial conditions for the full affine optimization procedure [1]. The mutual information metric for images I and J is given by

$$MI(I, J) = \frac{H(I) + H(J)}{H(I, J)}, \tag{3.4}$$

where $H(I)$ is the entropy of image I, and $H(I, J)$ is the joint entropy of images I and J. The entropy of an image is described by

$$H(I) = -\sum_i p_I(i) log(p_I(i)), \tag{3.5}$$

where $p_I(i)$ is the probability of a pixel having value i in image I, also known as a normalized histogram. The joint entropy of two images is given by

$$H(I, J) = -\sum_{i,j} p_{I,J}(i, j) log(p_{I,J}(i, j)), \tag{3.6}$$

where $p_{I,J}(i,j)$ is the probability of a pixel having value i in image I and value j in image J. This random trial stage is important because it reduces the effect of local minima in the affine optimization objective function between the histology images.

Registration parameters for the full affine stage are optimized using an intensity based mean squared error metric [12]. The implementation of the local registration algorithm also takes advantage of a multiresolution optimization scheme, which greatly reduces computation time in addition to improving the registration quality. Instead of optimizing the affine registration parameters on the 3DZM sized image regions (for this study, square regions of 650x650 pixels were used for each 3DZM) in a single stage, the optimization is broken into multiresolution stages. These stages begin by optimizing over decimated images, and slowly add in the previously removed image data as the registration solution is neared. For the first stage, the registration parameters for two decimated images are estimated through optimization. Once that optimization is complete, the parameters are passed as an initial guess to the next stage, where more of the image data is included. Then the higher resolution images are registered using initial conditions from the previous stage for the optimization. The process is repeated until the full resolution images are registered. By starting with decimated images, the overall registration process improves its robustness to optimization errors involving nonglobal extrema in the optimization function. Additionally, the initial alignments, which are furthest from the global solution, are computed with reduced data sets. This allows for fast convergence to an area near the global solution, and the higher resolution stages, which are computationally the most complex, will begin very close to their solution and converge in only a few iterations.

After the tissue sections are geometrically realigned, the photometric properties of the tissue must be equalized. Slight variation in the thickness of each section results in varying uptake of the H&E stain. This artifact of the slide preparation process is corrected by matching the first-order color statistics of each image in the set to a reference. For a warped

image I' and a true image I, the photometric deformation model is given by

$$I'(\mathbf{x}) = cI(\mathbf{x}) + d, \tag{3.7}$$

where c is the first-order, and d is the zeroth-order photometric change. Using this model, both the mean and variance of each individual color field (RGB) are scaled to match the reference values. The recovered true image for a single color field is given by

$$\hat{I} = \frac{\sigma_{ref}}{\sigma_{I'}}(I'(\mathbf{x}) - \mu_{I'}) + \mu_{ref}, \tag{3.8}$$

where $\mu_{I'}$ and $\sigma_{I'}$ are the mean and standard deviation of the warped image, and μ_{ref} and σ_{ref} are the reference values, which are equal to the average mean and average standard deviation across all warped images, respectively.

Following the registration and photometric adjustment steps, the computed transformations are applied to each image and a volume is assembled. However, 10-15% of the tissue sections are inadvertently damaged during the normal histology process. This is a result of sections being torn, folded over onto themselves, or otherwise lost. This renders the data from these damaged sections unusable. The missing sections must be filled in to complete the reconstruction of the tissue volume. The missing sections are replaced by interpolation, using cubic Hermite interpolation along each stacked column of pixels and independently for each color field [1]. Figure 3.3 shows a rendered 3D histology volume after all slices have been aligned and lost data has been interpolated.

3.4 Acoustic Impedance Assignment

Finally, each element of the tissue volume must be assigned an acoustic impedance value. This is accomplished based on the color value of the pixel, because the H&E staining causes

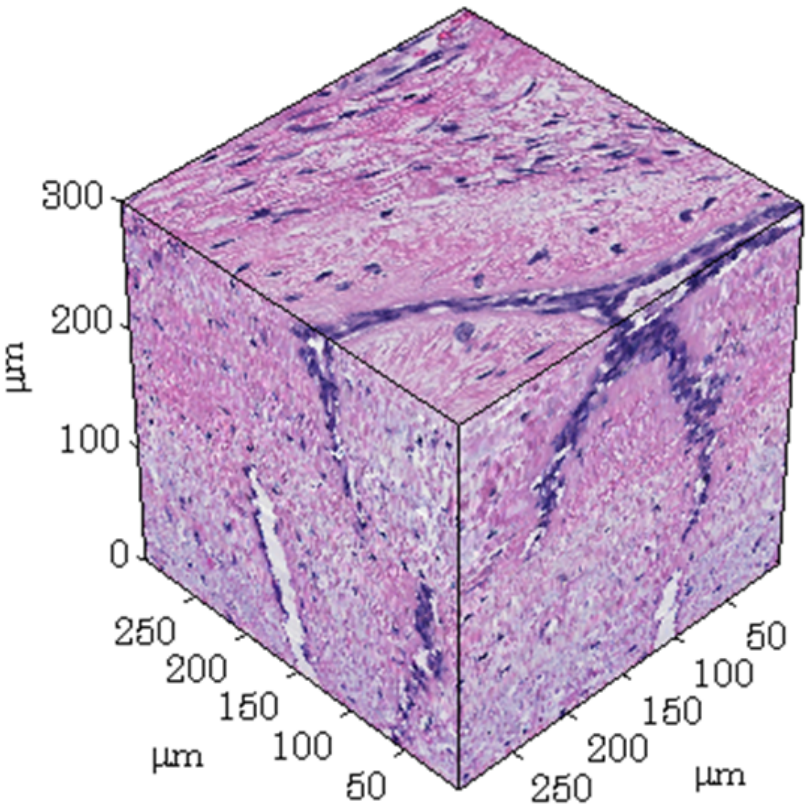

Figure 3.3: Rendering of 3D histology volume.

Table 3.1: Acoustic Impedance Assignment Scheme

Color	Tissue Component	Impedance Value Range
Light to Dark Pink	Cytoplasm	1.5 - 1.7 Mrayl
Light to Dark Blue	Cell Nuclei	1.8 - 2.0 Mrayl
White	Fat	1.45 Mrayl

tissue with a greater protein concentration to appear pink and tissue with a greater nucleic acid concentration to appear blue, thus differentiating the underlying tissue components. Impedance values were assigned by associating appropriate acoustic impedance values for each tissue structure with certain color ranges [1]. Tissue areas with eosin staining (indicating protein concentration) range in color from light pink to dark pink, while tissue areas with hematoxylin staining (indicating nucleic acid concentration) range in color from light blue to dark blue. For this work, it was assumed that the pink image elements represented cell cytoplasm, while the blue image elements represented cell nuclei. Each tissue structure was assigned a bulk materials impedance value, which was then increased or decreased proportionally to the amount of color saturation in each pixel. Other image elements which appeared very light or white were assumed to be fat. Thus, impedance values were assigned based on image color as indicated in Table 3.1. Figure 3.4 shows a rendered 3DZM after all pixels from the histology volume have been converted to acoustic impedance values.

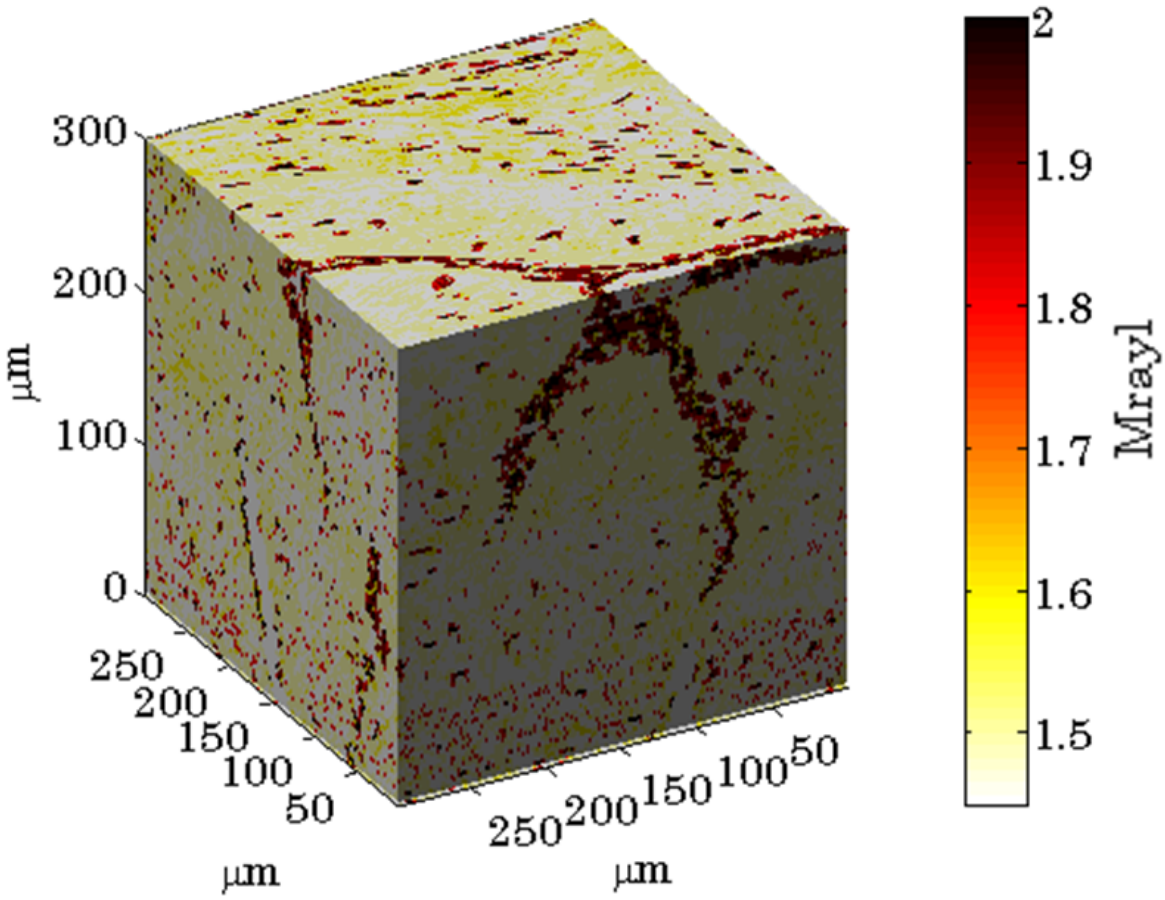

Figure 3.4: Rendering of a human fibroadenoma 3DZM.

Chapter 4

Impedance Map Analysis

4.1 3DZM Power Spectrum Estimation

As a result of the relationship between backscattered intensity and the squared magnitude of the spatial Fourier transform of a medium's relative impedance distribution, 3DZMs present a useful tool for the study of ultrasonic scattering in tissue. This relationship can be exploited in two ways. First, by assuming some form factor model, an estimate of the ESD in the 3DZM can be obtained. Second, by using the 3DZM to investigate the layout of the tissue microstructure from an acoustic perspective, new scattering models may be developed which help in physical scatterer identification and better represent the underlying tissue structure.

Spectral Estimation

Spectral estimation refers to the signal processing steps taken to compute an estimate of the Fourier transform of the 3D autocorrelation (power spectrum) of a 3DZM. In this step, the underlying tissue is treated as a random medium, for which it is desired to estimate the statistical power spectrum using the limited spatial samples of the volume.

The 3D spatial Fourier transform of a volume produces a 3D function of the spatial

frequency vector $\boldsymbol{k} = k_x\hat{x}+k_y\hat{y}+k_z\hat{z}$. In the special case of a spherically symmetric scatterer, the Fourier coefficients along each radial path away from $\boldsymbol{k} = \vec{0}$ are equal, regardless of which path is chosen; thus, the value of the 3D spatial Fourier transform along any such path is equal to the acoustic form factor of the medium, with the wave number $k = \sqrt{k_x^2 + k_y^2 + k_z^2}$. For an M-by-N-by-P element 3D volume $f(x, y, z)$, the 3D spatial discrete Fourier transform is given by

$$F(k_x, k_y, k_z) = \frac{1}{MNP} \sum_{x=0}^{M-1} \sum_{y=0}^{N-1} \sum_{z=0}^{P-1} f(x, y, z) \cdot e^{-j(k_x x+k_y y+k_z z)}. \tag{4.1}$$

Using (4.1), a discretized version of the 3DZM power spectrum from (2.4) is given by

$$F(k_x, k_y, k_z) = \left| \frac{1}{MNP(k_x^2 + k_y^2 + k_z^2)} \sum_{x=0}^{M-1} \sum_{y=0}^{N-1} \sum_{z=0}^{P-1} \frac{z(x, y, z) - z_0}{z_0} e^{-j(k_x x+k_y y+k_z z)} \right|^2. \tag{4.2}$$

Coherent scattering adds random variation to the underlying scattering function [6]. Coherent scattering arises from correlations among the inhomogeneities inside the impedance volume. This term is spatially dependent, so different radial paths of the 3D spatial Fourier transform will have different coherent scattering terms. By comparing the 3D power spectrum of a 3DZM to the 3D theoretical form factor given by (2.10), many radial paths are implicitly considered. This serves to reduce the effects of the coherent scattering term during ESD estimation. The weighting term $\frac{1}{(k_x^2+k_y^2+k_z^2)}$ in (4.2) is necessary because the number of samples in the discrete 3D power spectrum corresponding to a given spatial frequency magnitude $k = \sqrt{k_x^2 + k_y^2 + k_z^2}$ is proportional to the surface area of a sphere with radius k. Without this factor, a disproportionate amount of weight is placed upon high spatial frequency samples during ESD estimation. If improperly weighted, the ESD estimation process will tend toward matching correlation lengths that are not representative of the dominant

acoustic scattering structures within the volume.

In addition to weighting the power spectrum, the form factor must also be weighted by the same $\frac{1}{(k_x^2+k_y^2+k_z^2)}$ term. As a result, when using the full 3D power spectrum for ESD estimation, the fluid-filled sphere FF must take the form

$$F(k,d) = \frac{1}{k^2}\left(\frac{3j_1(kd)}{kd}\right)^2 = \left(\frac{3j_1(kd)}{k^2 d}\right)^2. \tag{4.3}$$

4.2 ESD Estimation

ESD estimation is the task of fitting a theoretical FF to the calculated power spectrum of a 3DZM (see Appendix). FFs of spherically symmetric scatterers, like the fluid-filled sphere FF described by (2.10), have a scatter size dependent frequency response. The ESD estimate for a 3DZM is calculated as

$$\hat{d} = \left(\underset{d\in[d_{min},d_{max}]}{\operatorname{argmin}} \sum_{k_x}\sum_{k_y}\sum_{k_z} |F_{3DZM} - F_{Theo}(d)|^2\right), \tag{4.4}$$

where F_{3DZM} is the power spectrum calculated from the 3DZM and $F_{Theo}(d)$ is the theoretical FF as a function of the effective scatterer diameter d. The constraint on the size of d is a result of the size and sampling frequency of the 3DZM. The minimum allowable diameter must be chosen large enough to limit the effects of the original histology image resolution and quantization noise on the estimated diameter. The maximum allowable diameter must be chosen to allow for accurate resolution in the frequency domain for a good estimate of (4.4). The frequency resolution of the discrete Fourier transform used to calculate F_{3DZM} is given by $1/(NT)$, where N is the number of samples and T is the sampling period in a given direction through the volume. Because the frequency profile of a typical FF narrows as d increases, the falloff region of the FF may be drastically undersampled for large ESD

estimates. This falloff region is the predominant feature of most FFs, and an undersampling of this region can greatly affect the robustness of (4.4). For this study, the allowable range for $\hat{d}$ was set as 10 μm to 180 μm. This chosen range forces all ESD estimates to be large with respect to a pixel size, yet small enough to allow for an accurate and robust formulation of (4.4).

Chapter 5

ESD Simulation

5.1 Computational Phantom

Prior to this work, ESD estimation made an assumption of tissue isotropy. Under isotropy, all radial paths through the three-dimensional power spectrum of the 3DZM are equivalent. This assumption simplifies (4.1) into a one-dimensional Fourier transform in a given direction. This simplification reduces the computational complexity of computing the power spectrum of a 3DZM, as well as the fitting procedure (4.4). Many tissue types, like fibroadenoma, however, are highly anisotropic. In this work, the full three-dimensional power spectrum given by (4.2) is used for ESD estimation. To validate this choice, a synthetic 3DZM with known acoustic properties was used to evaluate the performance and computational complexity of both power spectrum estimation methods. A computational phantom of size 300x300x300 μm^3 was generated with 10 randomly placed spherical inclusions of diameter 60 μm. The background was set to an acoustic impedance of 1.6 Mrayl and the scatterers were set at 1.8 Mrayl. Figure 5.1 shows the spherical inclusions inside the synthetic 3DZM.

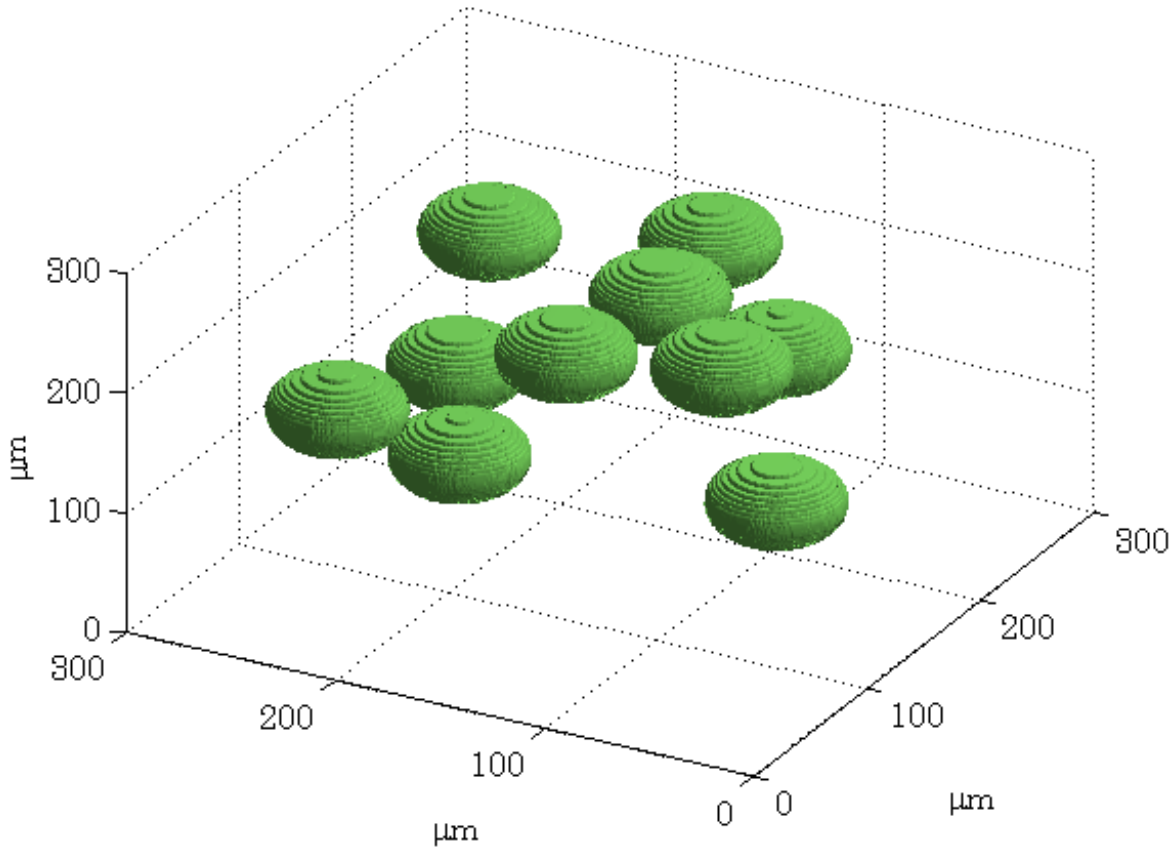

Figure 5.1: Spherical inclusions of diameter 60 μm inside the computational phantom.

5.2 ESD Results

The ESD was estimated with both methods. The method with the isotropy assumption estimated ESD as 180 μm. The fitting error as a function of ESD can be seen in Figure 5.2. The duration of the estimation process was 3.78 seconds. The three-dimensional power spectrum estimation method of this study estimated the ESD as 74 μm. The fitting error as a function of ESD can be seen in Figure 5.3. The duration of the improved estimation process was 24.18 seconds. The computational phantom provided a difficult estimation target due to the close proximity of the inclusions within the volume. The previous estimation method

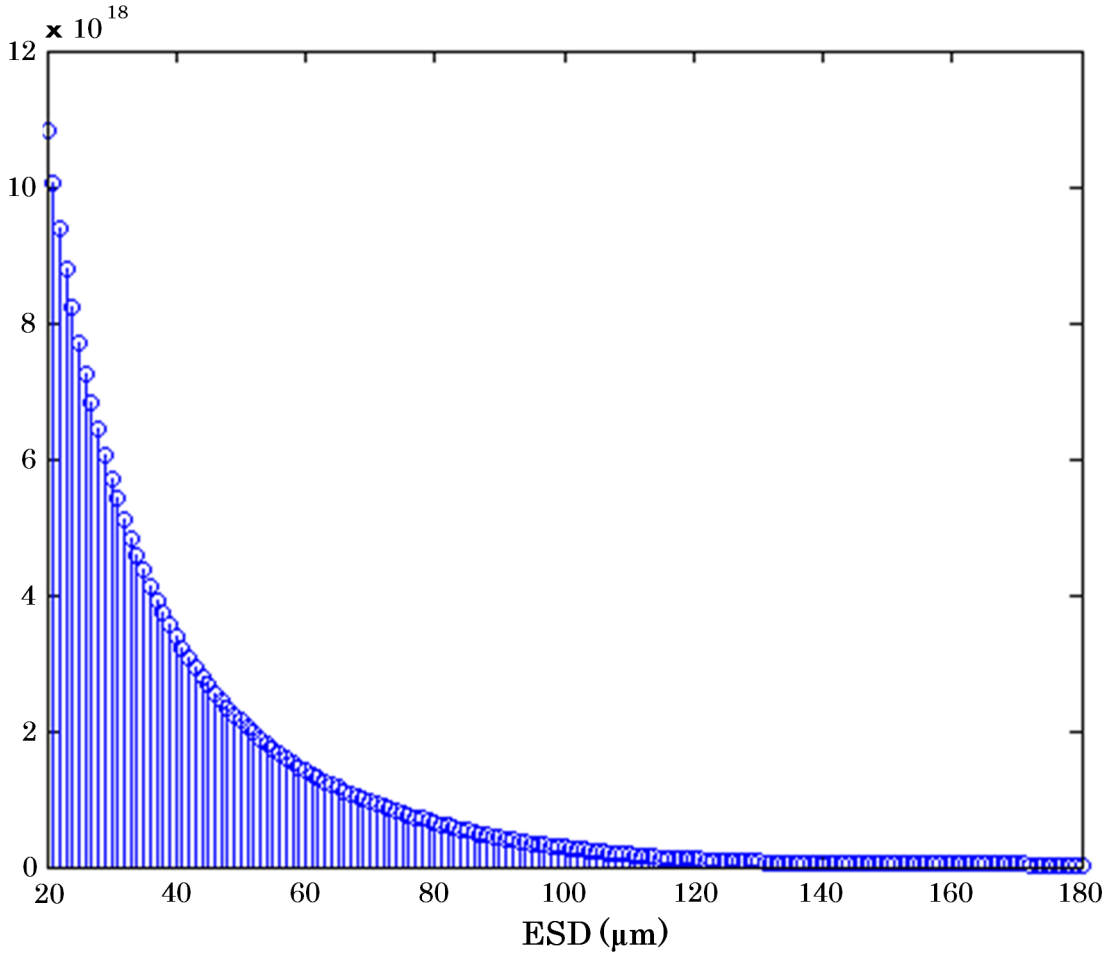

Figure 5.2: FF fitting error as function of ESD with isotropy assumption.

produced an unusable result, while the method of this study produced a much closer estimate at only a modest increase in computational resource requirements.

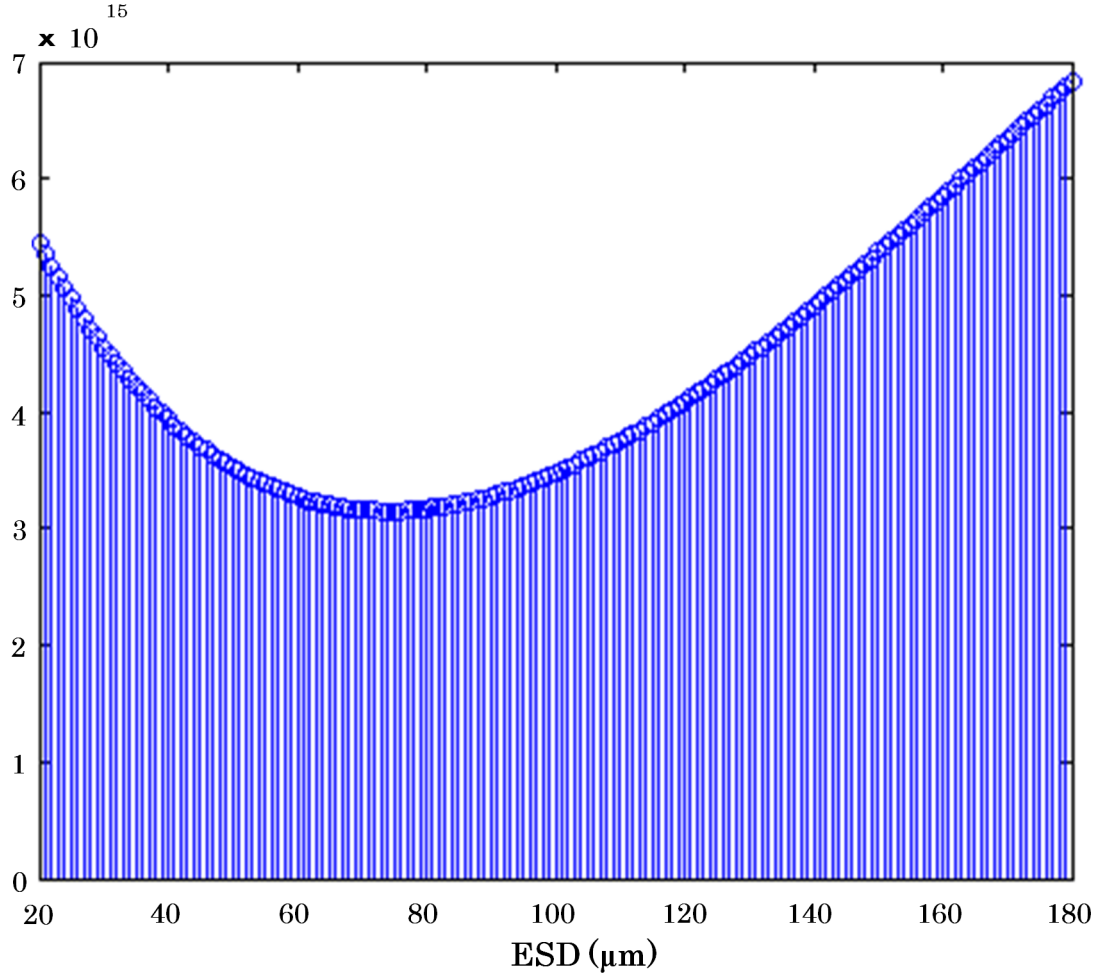

Figure 5.3: FF fitting error as function of ESD without isotropy assumption.

Chapter 6

Human Fibroadenoma Study

6.1 Fibroadenoma ESD Estimates

3DZMs were constructed and analyzed for 33 independent human fibroadenoma data sets. No additional information about each data set was known other than the fact that each was pathologically identified as fibroadenoma, i.e., no ultrasonic scan data were available for the samples. For each data set, one 300x300x300 μm^3 3DZM was created. The power spectrum of each 3DZM was estimated, and a scattering model was applied in order to extract ESD parameters. The scattering model used for analysis was the fluid-filled sphere FF in (2.10).

Across all 33 data sets, the average estimated ESD for the 300x300x300 μm^3 3DZMs was 111.4$\pm$40.7 μm. Figure 6.1 shows a histogram of the ESD estimates obtained for the human fibroadenoma data sets.

The histogram in Figures 6.1 shows a large spread in the ESD estimates across different data sets. Different fibroadenoma samples, however, show a wide variety of structure shapes and sizes. Figure 6.2 shows two tissue sections from two independent fibroadenoma data sets. In each figure, the acini, or duct-like dark structures through the tissue, take drastically different forms. A highly varying set of ESD estimates is expected for tissue with a great

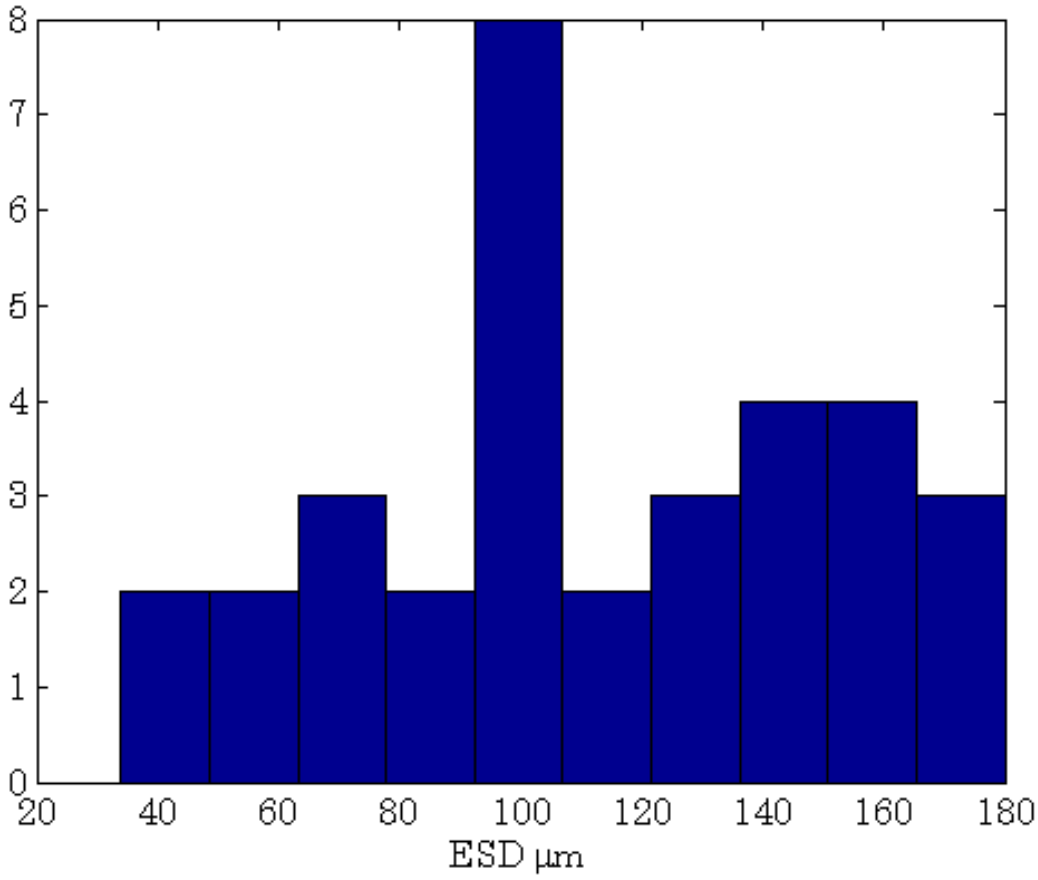

Figure 6.1: Histogram of ESD estimates obtained from 33 human fibroadenoma 300x300x300 μm^3 ROIs.

deal of high level structure, like fibroadenomas.

6.2 Volume Segmentation

Figures 6.3, 6.4, and 6.5 show a segmentation of the high and low impedance structures inside three of the human fibroadenoma 3DZMs in this study. The enclosed green structures represent the high impedance tissue inside of the lower impedance background tissue. Anatomically, this is a separation of the acini and duct structures from the stroma, or surrounding structural tissue.

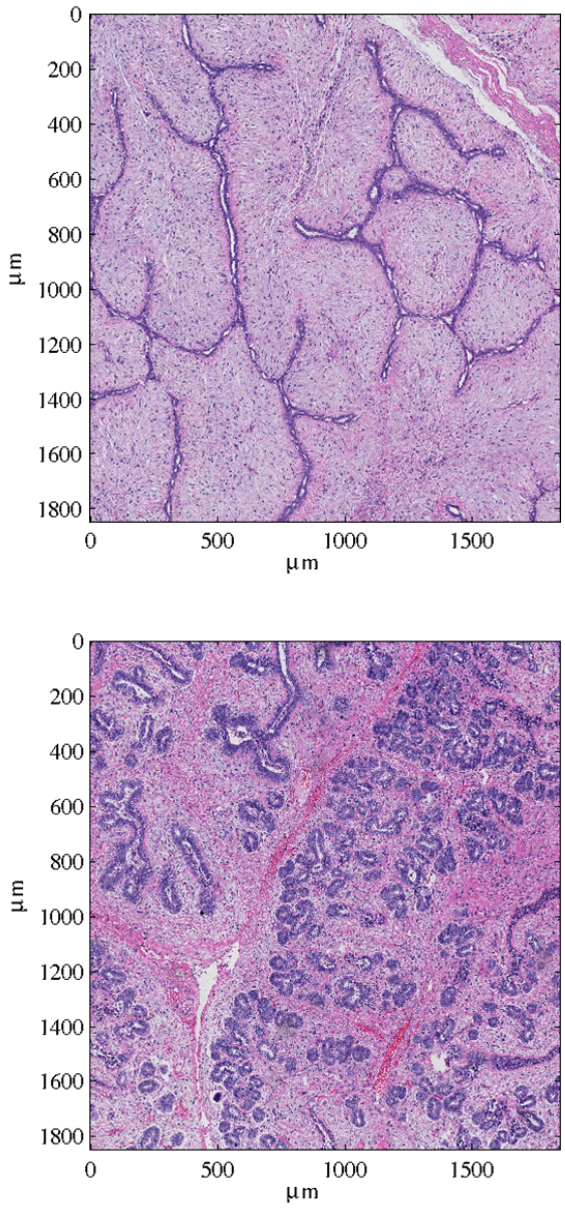

Figure 6.2: Sections from two independent fibroadenoma tissue samples.

For the data set in Figure 6.3, the ESD for the 300x300x300 μm^3 3DZM was 127 μm. For this data set, distinct structures of a size that visually corresponds to ESD estimates can be observed inside the volume (see Appendix).

For the data set in Figure 6.4, the ESD for the 300x300x300 μm^3 3DZM was 70 μm.

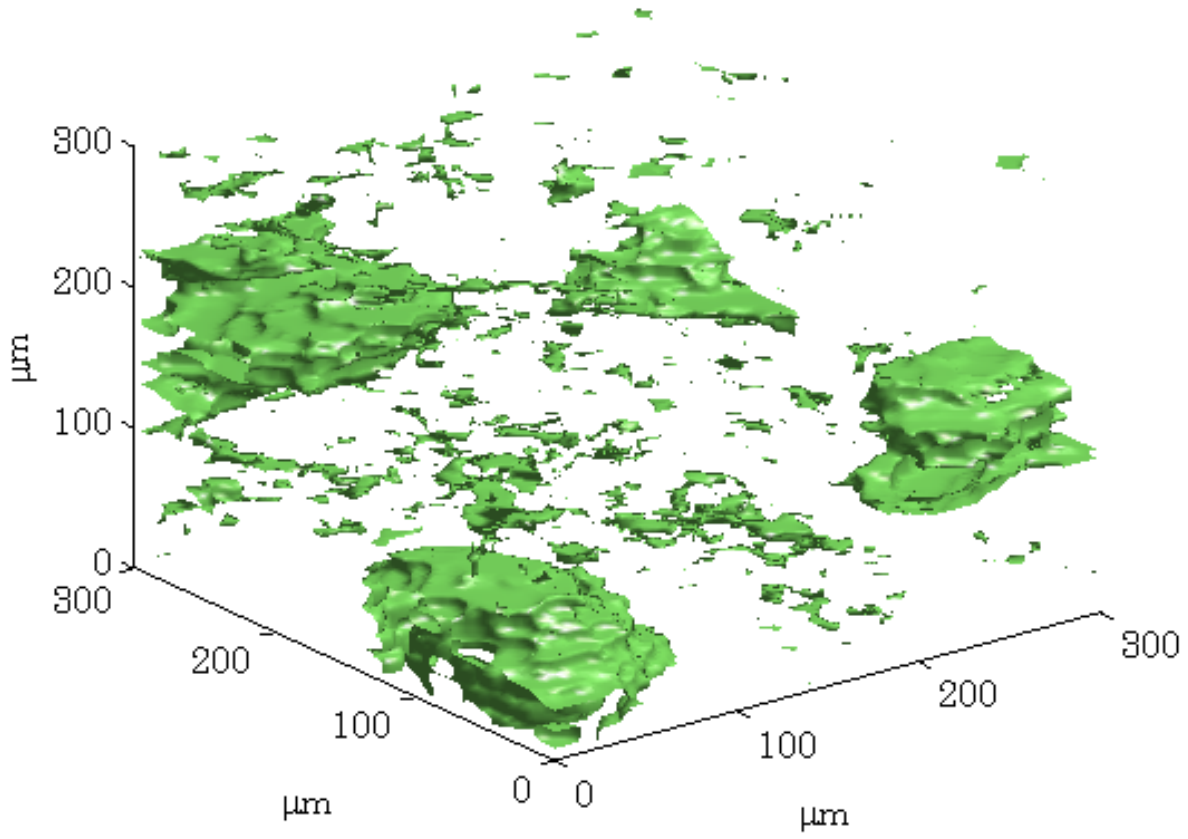

Figure 6.3: Segmentation of high and low impedance structures. ESD estimate for this 3DZM is 127 μm.

There are no spherical scattering bodies inside this data set with the estimated ESD. The sheet-like structure inside the volume is matched poorly by the fluid-filled sphere scattering assumption made in this study. As a result, the ESD estimates give little intuition as to the tissue microstructure for this data set. In this case, the 3DZM method shows that a simple scattering model like the fluid-filled sphere FF may be inadequate for characterizing highly structured tissue.

For the data set in Figure 6.5, the ESD for the 300x300x300 μm^3 3DZM was 99 μm. For this data set, the segmentation shows densely packed inclusions. While individual inclusions

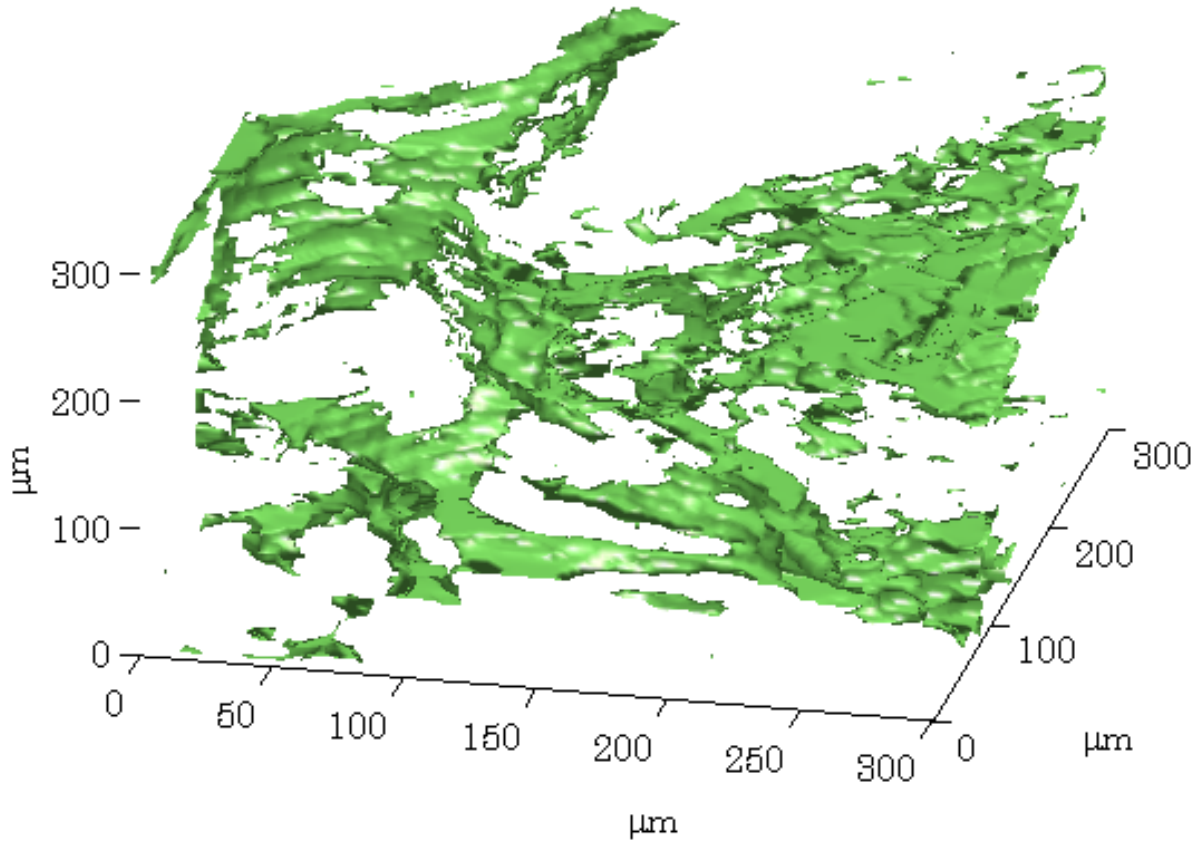

Figure 6.4: Segmentation of high and low impedance structures. ESD estimate for this 3DZM is 70 μm.

are smaller than the estimated ESD, the clusters of inclusions are of a size in moderate agreement with the ESD estimates. Although there is not a direct link between ESD estimates and specific inclusions in a data set, the agreement between ESD estimates and anatomical segmentation images, especially when the segmented inclusions are spherically shaped (i.e. in agreement with the fluid-filled sphere scattering model), shows some of the potential of ESD as a tissue descriptor, and motivates further work on the topic.

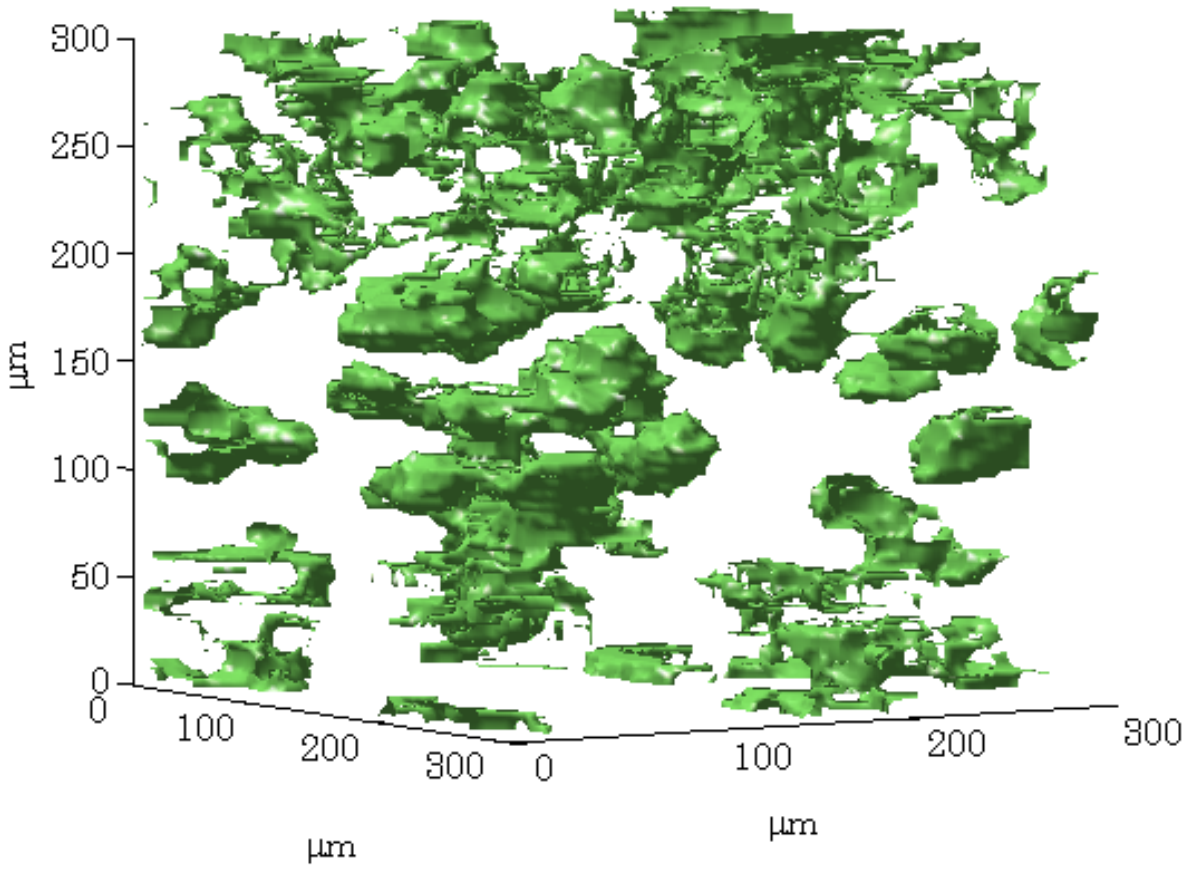

Figure 6.5: Segmentation of high and low impedance structures. ESD estimate for this 3DZM is 99 μm.

Chapter 7

3DZM and QUS Analysis of Rabbit Liver

The most important question remaining about 3DZMs is their validity as acoustic tissue models. The ultimate goal of 3DZM development is to provide a computational environment where important small scale scattering techniques and parameters can be implemented and evaluated. The success of this goal is tied to the strength of the link between 3DZM and QUS techniques. In order for information gleaned from 3DZMs to be applicable in the QUS domain, the relation between the two must be well quantified. In order to examine the link between 3DZM and QUS techniques, the following experiment was developed.

7.1 Experiment Overview

Starting from a single piece of tissue (rabbit liver was used for this experiment), the ESD was estimated using both QUS and 3DZM techniques. A block diagram for the experiment is shown in Figure 7.1. First, a sample of rabbit liver was chemically fixed using formalin. After fixation, the sample was ultrasonically scanned. After scanning, the sample was prepared

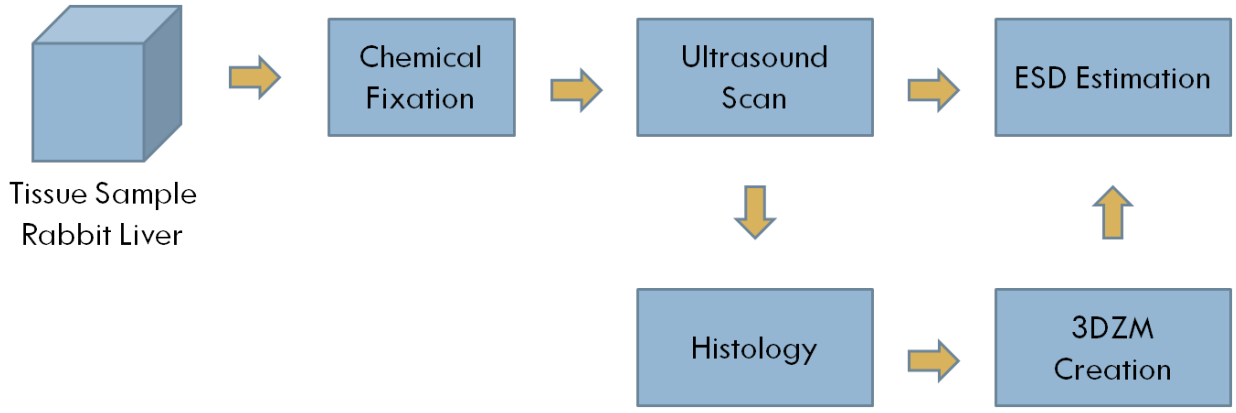

Figure 7.1: Rabbit liver experiment block diagram.

into 400, 3 μm thick histology sections. Each section was stained with H&E dye. From this single set of sections, 24 3DZMs were constructed. Finally, ESD was estimated using the ultrasonically acquired data and the 3DZM data independently, and the results were compared. The key innovation of this experiment is that the ultrasound scan occurs after, instead of prior to, chemical fixation. This allowed for a much more reliable comparison of the ultrasound data with the 3DZM data, as the change in acoustic properties of the tissue caused by chemical fixation does not have to be corrected for when comparing the data acquired from the two separate modalities.

7.2 Tissue Sample Selection

The tissue used in this experiment was a sample of rabbit liver. Liver was chosen because of its homogeneity. It is composed of hepatocyte cells, the nuclei of the hepatocyte cells, and vasculature. Since the liver has very little to no high level structure, the tissue is nearly isotropic, specifically when viewing with a large ROI with respect to the hepatocyte cell size. Under these conditions, the assumption was made that the ESD estimation process was independent of both direction and location.

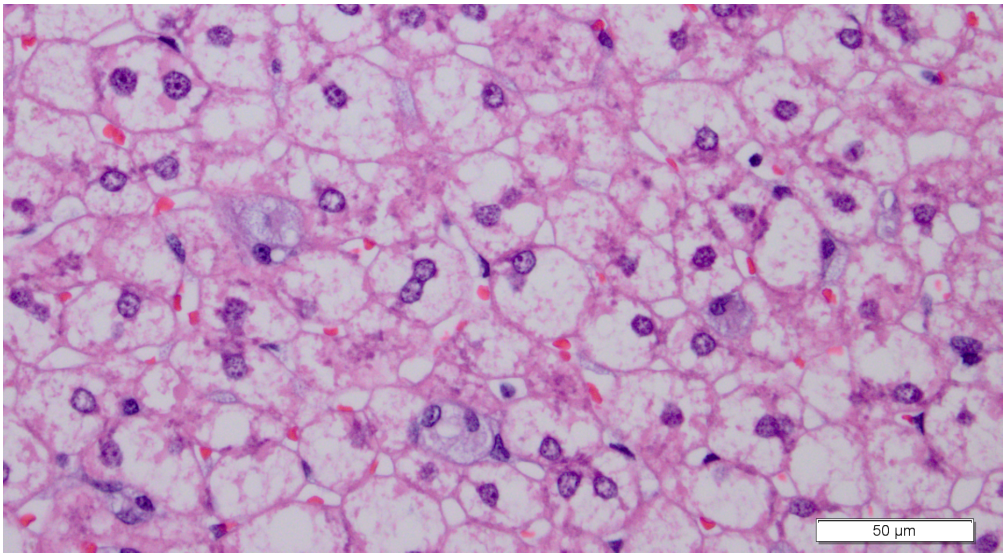

Figure 7.2: Rabbit liver histology sections.

Two histology sections of the rabbit liver are shown in Figures 7.2 and 7.3. As can be seen, the hepatocyte cell size is typically 30-40 μm in diameter. The nuclei are approximately 7-8 μm in diameter. The relative homogeneity and simplicity of these samples makes them appealing targets for an experiment comparing different modalities.

7.3 Ultrasonic Data Acquisition

As stated previously, ultrasonic data were acquired from the chemically fixed section of liver tissue. The data were collected over a wide frequency range, using multiple ultrasonic transducers. Table 7.1 contains the pertinent information about the ultrasonic transducers used in this experiment.

Figures 7.4 and 7.5 show B-mode slices taken from the chemically fixed rabbit liver sample. Figure 7.4 was acquired with the 7.5 MHz center frequency transducer. Figure 7.5 was acquired with the 20 MHz center frequency transducer.

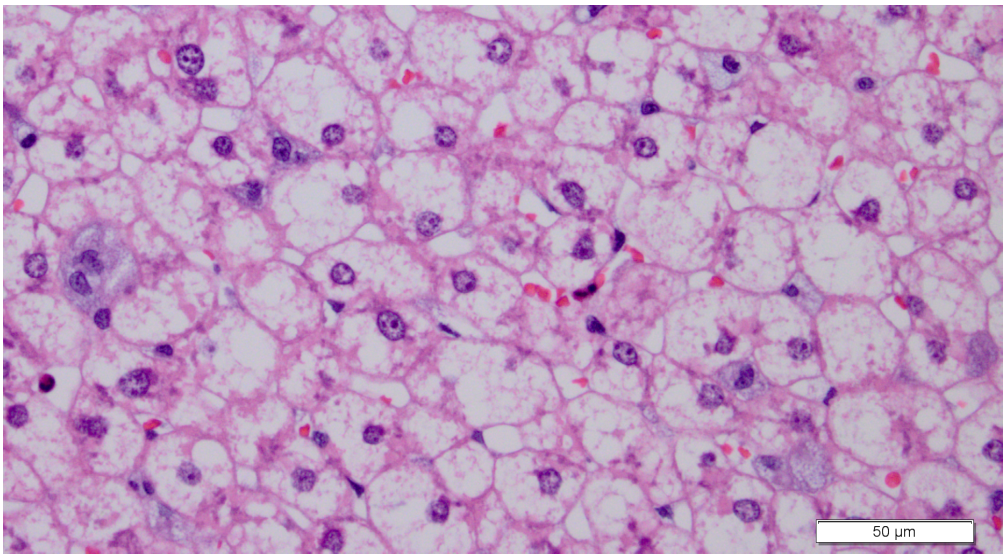

Figure 7.3: Rabbit liver histology sections.

Table 7.1: Ultrasonic Transducer Properties

Center Frequency	F Number	Bandwidth	Fractional Bandwidth
7.5 MHz	4	3.26 MHz (3 dB)	42% (3 dB)
13 MHz	3	5.10 MHz (3 dB)	38% (3 dB)
20 MHz	3	5 MHz (3 dB)	33% (3 dB)
40 MHz	3	40 MHz (10 dB)	100% (10 dB)
65 MHz	3.5	40 MHz (10 dB)	62% (10 dB)

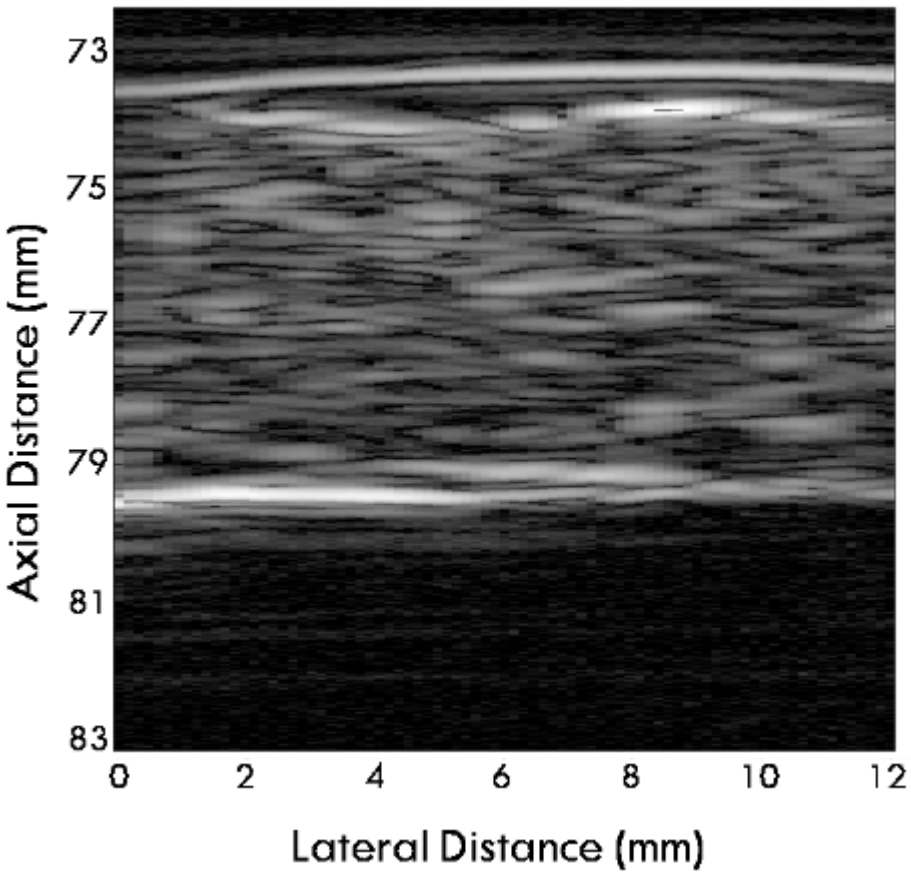

Figure 7.4: B-mode image taken with 7.5 MHz center frequency transducer.

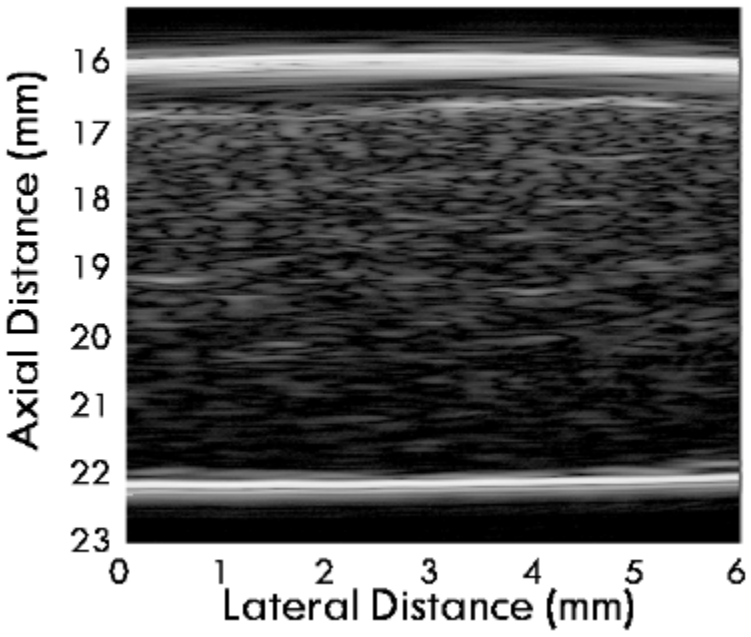

Figure 7.5: B-mode image taken with 20 MHz center frequency transducer.

7.4 3DZM Technique

Twenty-four 3DZMs were constructed from the histology section set acquired from the rabbit liver. The 3DZMs created are 300x300x300 μm^3 in volume, and have a voxel size of 0.46x0.46x3 μm^3. The locations in the histology chosen to construct each 3DZM were selected in order to avoid areas of vasculature. Figure 7.6 shows the reconstructed histology volume for a 300x300x300 μm^3 portion of the liver sample. Figure 7.7 shows a histology section that has been converted into acoustic impedance values. As can be seen, the nuclei have been assigned a higher acoustic impedance value than the surrounding tissue. Figure 7.8 shows one of the 300x300x300 μm^3 3DZMs created from the rabbit liver sample.

The ESD was estimated for 3DZMs using two separate methods of power spectrum estimation. First, the power spectrum is estimated by the standard formula (4.2). In addition

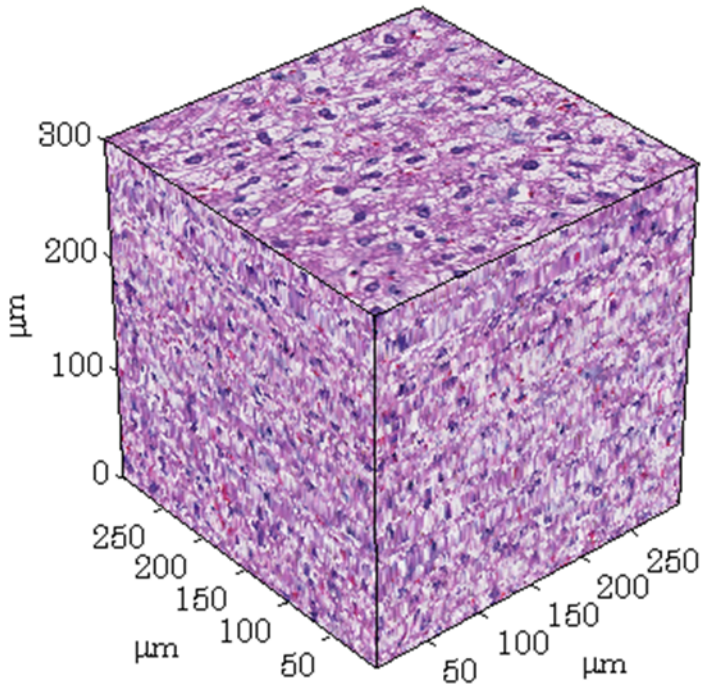

Figure 7.6: 3-D histology block constructed from rabbit liver.

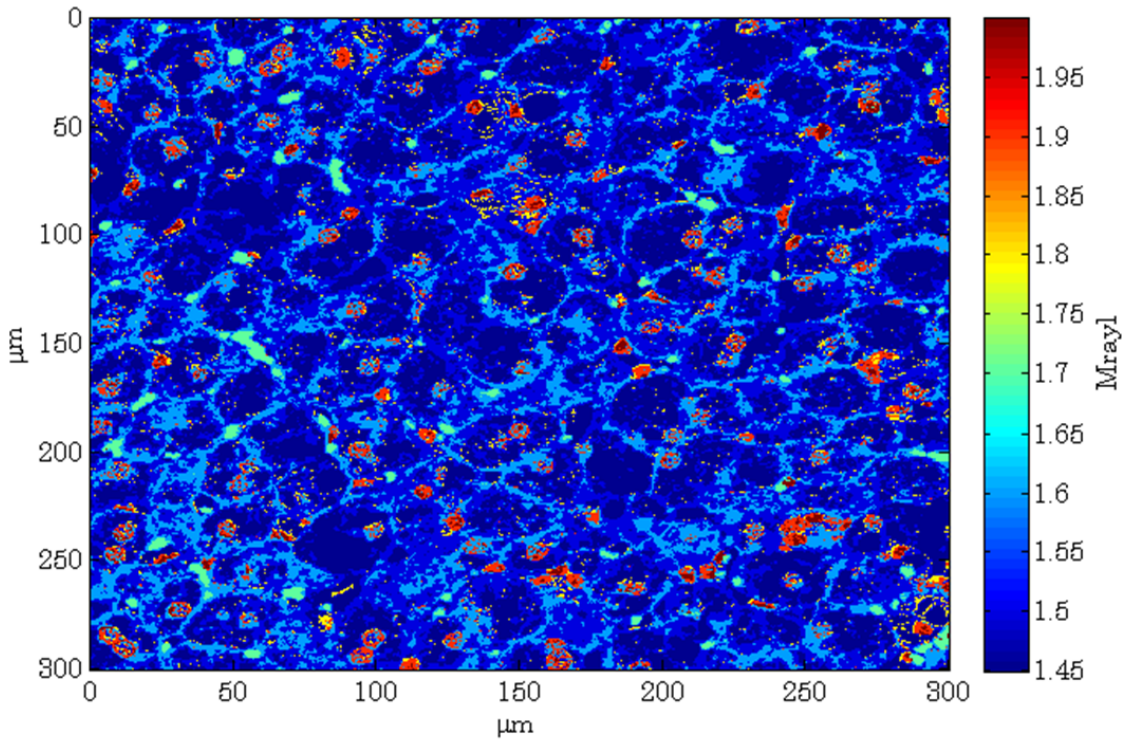

Figure 7.7: 2-D slice of acoustic impedance values from rabbit liver.

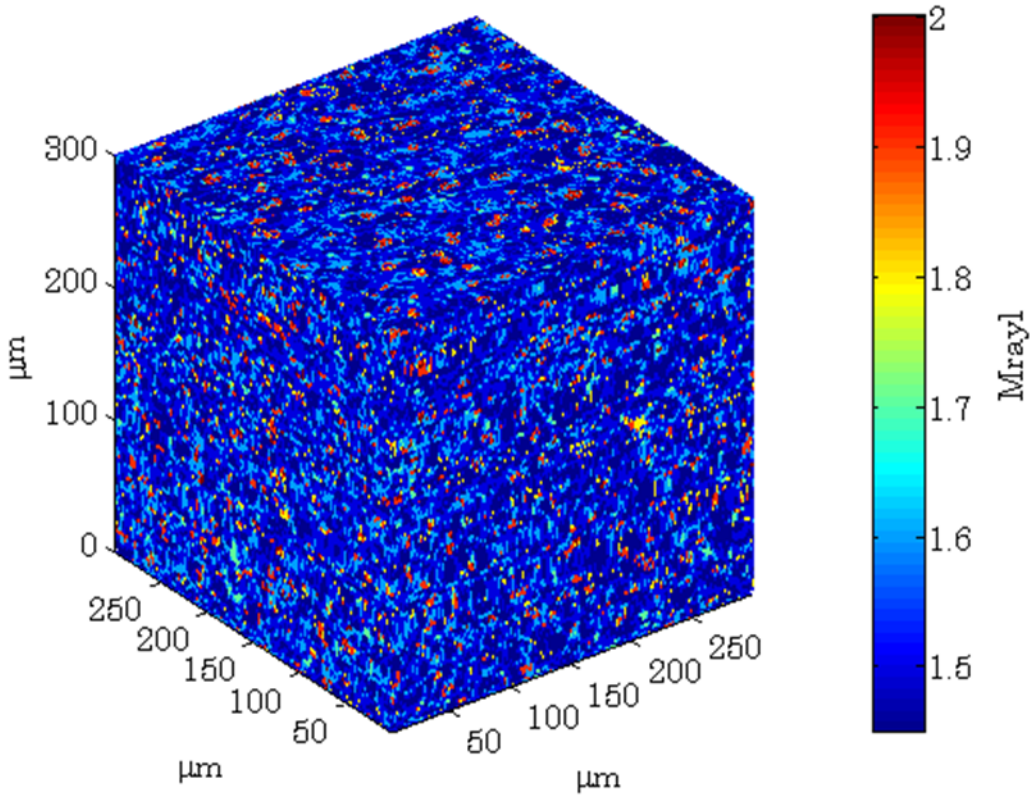

Figure 7.8: 3DZM constructed from rabbit liver sample.

to this, a second, weighted, power spectrum is estimated by

$$F(k_x, k_y, k_z) = \left| \frac{1}{MNP} \sum_{x=0}^{M-1} \sum_{y=0}^{N-1} \sum_{z=0}^{P-1} \frac{z(x,y,z) - z_0}{z_0} e^{-j(k_x x + k_y y + k_z z)} \right|^2 . \tag{7.1}$$

This equation differs from (4.2) in the fact that it does not include the $\frac{1}{(k_x^2+k_y^2+k_z^2)}$ term. This power spectrum, when compared to a suitable form factor (given by (2.10) for this experiment), provides an implicit weighting of the ESD estimation process toward smaller ESD sizes. This was done in an effort to emphasize smaller scatterers and extract a smaller ESD estimate. Both the standard power spectrum (4.2) and the weighted power spectrum (7.1) were used to estimate ESD for all 24 rabbit liver 3DZMs.

7.5 ESD Results

ESD was estimated independently for the ultrasound and the 3DZM portions of the rabbit liver experiment. Table 7.2 shows the mean and standard deviation of the ESD estimates for the 24 3DZMs. Table 7.3 shows the mean and standard deviation for all 5 transducers of the QUS ESD estimates obtained by the method in [13].

For the 3DZMs, the different optimization weightings produce very different ESD estimates. With the standard method, the ESD estimate is 93.6±52.7 μm. The mean value corresponds visually to the size of a small cluster of hepatocyte cells. The large standard deviation, however, suggests that the estimated power spectra are not strongly tied to a single ESD size.

For the weighted optimization ESD estimation, the ESD is 7.04±1.30 μm. This size is significantly smaller than the ESD estimates from the standard method, as is expected by the additional weight put on high frequency FF matching. The average value of 7.04 μm corresponds visually to the size of a single nucleus. Although there is no strong link between

Table 7.2: ESD Estimates for Rabbit Liver 3DZMs

3DZM Power Spectrum	Standard	Weighted
ESD (μm)	93.6±52.7	7.04±1.30

Table 7.3: ESD Estimates for Rabbit Liver Backscatter

Transducer	7.5 MHz	13 MHz	20 MHz	40 MHz	65 MHz
ESD (μm)	102.2±30.5	63.3±12.2	23.6±26.2	19.8±1.1	2.78±6.43

ESD and physical structures (see Appendix), the low standard deviation of the ESD estimates shows that the fluid-filled sphere FF of approximate size 7 μm is the optimal fit for the vast majority of 3DZMs created from the rabbit liver sample.

For the ultrasound backscatter data, the general trend is observed that the ESD estimate becomes smaller with increasing center frequency transducers. This is an expected trend, as the maximum sensitivity of ultrasound to small-scale scatterers occurs around $ka = 1$. The ESD estimates from the 3DZMs fall in between the ESD estimates for the 7.5 MHz and 13 MHz (average sizes of 102.2 μm and 63.3 μm) for the standard 3DZM ESD estimation, and between the ESD estimates for the 40 MHz and 65 MHz (average sizes of 19.8 μm and 2.78 μm) for the weighted 3DZM ESD estimation.

7.6 Non-normalized Form Factor Comparison

Although the comparison of ESD estimates from 3DZMs and ultrasonic backscatter showed that 3DZMs can produce ESD estimates that fall inside the ESD estimates from QUS techniques over a reasonable frequency range, simply looking at ESD estimates does not provide a strong, quantitative link between general 3DZM methods and QUS methods. In an effort to begin exploring this link, the non-normalized FF between the two methods was compared. In [10], the ultrasound backscatter coefficient is shown to be proportional to the product of

spatial frequency raised to the fourth power and the Fourier transform of the 3D spatial autocorrelation of the relative acoustic impedance function. This relationship can be expressed as

$$\sigma_{bsc}(k) = Ak^4 \left| \iiint_V \frac{z(r) - z_0}{z_0} e^{-jkr} dV \right|^2, \tag{7.2}$$

where A is a proportionality constant. By using the 3DZM to generate the spatially varying impedance function, and ultrasonic backscatter to generate the backscatter coefficient, the two modalities can be compared in a more meaningful way than ESD estimates. By replacing the Fourier transform of the 3D spatial autocorrelation of the relative acoustic impedance function with the 3DZM power spectrum $F_{3DZM}(k)$, (7.2) becomes

$$\sigma_{bsc}(k) = Ak^4 F_{3DZM}(k). \tag{7.3}$$

By rearranging terms, the final form is

$$\frac{\sigma_{bsc}(k)}{k^4} = AF_{3DZM}(k), \tag{7.4}$$

where $\frac{\sigma_{bsc}(k)}{k^4}$ is the non-normalized FF generated from ultrasound backscatter. This term can now be compared to the power spectrum of a 3DZM through the proportionality constant A. Comparing the non-normalized FF to the 3DZM power spectrum is easier to interpret than comparing the backscatter coefficient to the product k^4 and $F_{3DZM}(k)$ because quantization error brought on by the voxel size of the 3DZM is amplified at high frequencies by k^4. That noise makes visual comparison very difficult, and as a result the non-normalized FF is used for this experiment.

Figure 7.9 shows an averaged 1D power spectrum from the 3DZMs. The spectrum was generated by averaging the power spectra in the k_x and k_y directions for all 24 3DZMs. Figure 7.10 shows the non-normalized FF from the ultrasound backscatter data. The data

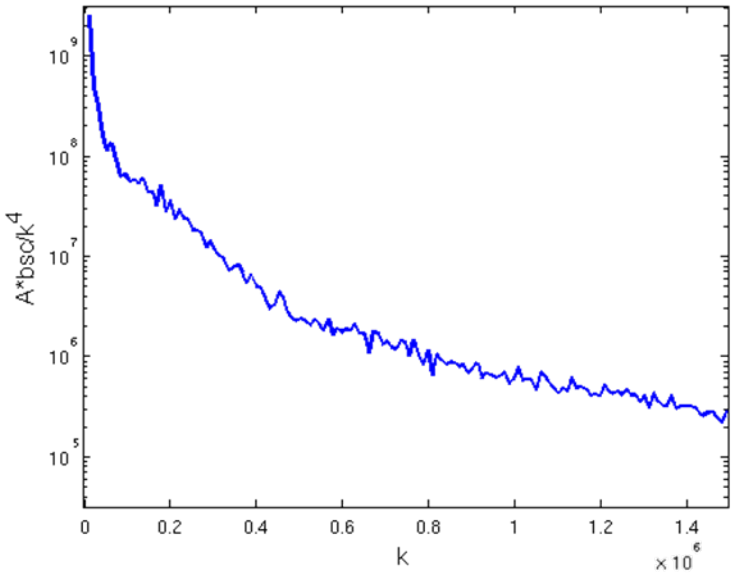

Figure 7.9: Product of proportionality constant and 3DZM power spectra.

are labeled below the figure according to the center frequency of the transducer used for that portion of data. Both figures have been plotted on a logarithmic scale. By doing so, the proportionality constant A becomes simply an offset.

As can be seen, apart from a y-axis offset, both modalities exhibit similar behavior. There is a similar dropoff of four to five orders of magnitude up to a spatial frequency of $1.5E6\frac{1}{m}$ for both modalities. That frequency value was used as the maximum value for the 3DZM power spectra because above that level, the power spectra are dominated by quantization noise from the 3DZM voxel size. The backscatter data from the 13 MHz transducer was problematic, and appears to be an outlier, but was included in this study for the sake of completeness.

The fact that the general shape of the 3DZM and ultrasonically acquired data was qualitatively so similar is very promising for future work. Despite some of the problems that arose during this experiment (detailed in the next section), the estimated FF and ESD estimates for both modalities agreed relatively well. As the 3DZM continues to evolve as a

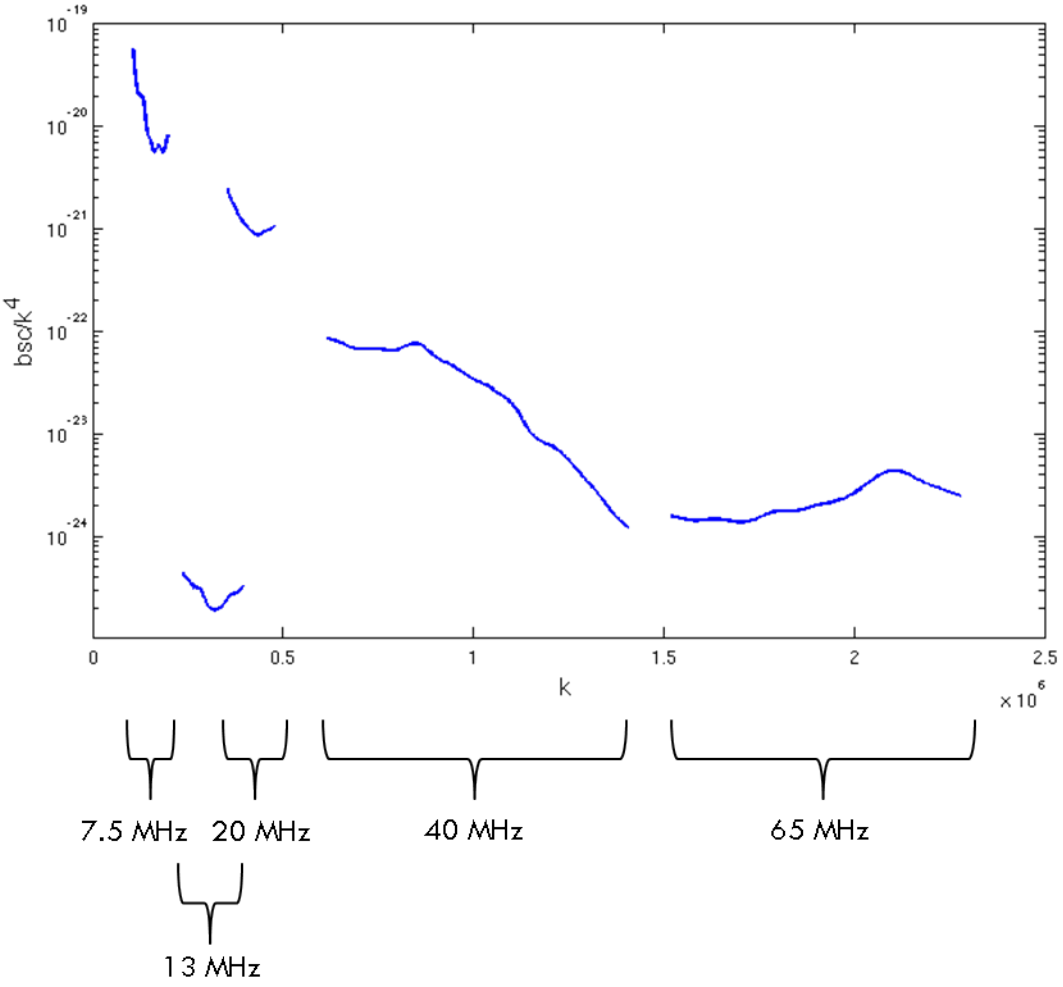

Figure 7.10: Non-normalized FF from backscatter data.

development tool for QUS techniques and parameters, the continued examination of the link between these two very different modalities will be critical in the creation and verification of new small-scale ultrasound imaging techniques.

7.7 Experimental Concerns

There were several issues that arose during this rabbit liver experiment that caused problems and severely limited the amount of quantitative comparison that could be done between the 3DZM based and the QUS based parameter estimation techniques. The first issue to note was that the rabbit liver used in this experiment was a fatty liver, not a healthy liver. The fatty liver has not been well characterized, and introduced additional heterogeneities that were not accounted for in the experiment.

In addition to the liver sample problem, there were several issues with the ultrasonic data acquisition. First, quality measurements of acoustic attenuation were not collected from the fixed liver sample. Instead, a value of 1 $\frac{dB}{cm \cdot MHz}$ was used. Errors in that attenuation value would affect the backscatter coefficient. Also, the data acquired from the 13 MHz transducer appeared to be a somewhat severe outlier. At the point when this issue was recognized, the rabbit liver sample had been sliced into histology sections, which ruled out the option of rescanning the tissue.

Even though these problems existed, the data from this experiment still gives promising results. Future experiments that can anticipate these issues certainly hold the potential to develop a complete and quantitative link between 3DZMs and QUS techniques.

Chapter 8

Conclusion and Future Work

8.1 Summary of Contributions

8.1.1 3DZM Construction

This work has improved 3D histology reconstruction both in terms of performance and cost. A robust, multiresolution registration scheme that uses multiple optimality metrics was developed. This new registration algorithm can accurately align histology slices, yet does not unnaturally deform the tissue sections or otherwise degrade the histology data set. New methods of photometric correction help to preserve E&H staining for a more faithful impedance assignment process than was possible with earlier methods based on histogram equalization. Also, automated removal of damaged histology sections helps to vastly improve the quality of the ultimate histology volume.

8.1.2 Human Fibroadenoma Study

The 3DZM technique was demonstrated on a set of 33 independent human fibroadenoma samples. The purpose of this study was twofold. First, it was an examination of the human

fibroadenoma. The 3DZM provides a unique ability of being able to study the fibroadenoma both visually using the 3D histology volume, and acoustically by extracting QUS parameters like ESD. Using both paths, this study found that human fibroadenomas contain a great deal of variability from patient to patient. The typical ranges for this variability, as well as identifying possible acoustic scattering sources, may prove to be a valuable discriminating characteristic as other tumor types are explored with the 3DZM method.

Additionally, this work had the purpose of examining the viability of the 3DZM as a useful tool. This human fibroadenoma study was the first large scale study completed with 3DZMs on real tissue. The ability of the 3DZM to both produce QUS parameters as well as segment the microstructure visually highlighted the strength of the 3DZM method. The success of this study will propel the 3DZM on to studies of different tissue types and new applications.

8.1.3 Rabbit Liver 3DZM/QUS Comparison

The comparison of 3DZMs and ultrasonic backscatter measurements via rabbit liver was a novel study that showed a potentially strong relationship between 3DZM and QUS techniques. Although this experiment had some issues, as nearly all new experiments do, the results were still very promising. ESD estimates from 3DZMs made from chemically fixed rabbit liver fell within the range of ESD estimates produced by ultrasonic backscatter from the same fixed rabbit liver using transducers that spanned from 7.5 to 65 MHz. Additionally, the 3DZM power spectrum and the non-normalized FF showed similar characteristics, which allows for the future optimization of 3DZM construction parameters in order to make the 3DZM as similar to real tissue as possible.

8.2 Future Work

8.2.1 3DZM Construction

The major element of 3DZM construction yet to be fully addressed is the assignment of acoustic impedance values. The key to truly developing a robust impedance assignment scheme lies in two areas. First and most importantly, ultrasound backscatter data must be utilized. In the rabbit liver experiment that compared 3DZM and QUS ESD estimation earlier in this work, it was shown that the power spectrum obtained from a 3DZM has a similar shape to the non-normalized FF obtained from ultrasonic backscatter. By considering the proportionality constant, which is heavily dependent on the acoustic impedance of the underlying tissue, between those two spectra, the impedance assignment scheme can be optimized for a best fit between the two spectra. Both the impedance value assigned to the E&H coloration and the levels of quantization for the impedance assignment can be optimized in order to bring the 3DZM as close as possible in an acoustic sense to real tissue.

The second element that will improve impedance assignment is to expand upon the H&E staining criterion for assigning impedances. Both new dyes and spatial features can be taken advantage of. Dyes that attach themselves to different tissue structures can differentiate tissue in ways that H&E staining cannot. Studying multiple dyes or finding a dye that best differentiates structures of differing acoustic impedances would certainly be beneficial. Using the spatial features of tissue could also improve the impedance assignment scheme. By using image processing and segmentation techniques, individual structures, such as nuclei, individual cells, or clusters of cells, could be identified in tissue. Once those individual structures are identified, the impedance assignment scheme for that structure can be appropriately chosen from a set of known tissue structure acoustic impedance ranges.

Although the histology section registration process has been greatly improved, the development of 3DZM would still benefit from a quantitative metric that assesses the feasibility

of the realigned histology. There is currently a disconnect in 3D histology reconstruction. When realigning real tissue according to some metric, such as mean squared error or mutual information, a strong set of matching registration parameters can be found, but these metrics do not take into acount the fact that the tissue anatomically changes from slice to slice as you move through the volume. To truly validate the reconstructed histology, a vital part to the use of 3DZMs, a metric should be used that assesses both alignment quality and tissue feasability, such as limits on tissue structure sizes and curvature.

8.2.2 Tissue Study

The ultimate goal of the 3DZM is to provide a convenient test bench in the computational domain for the development of QUS techniques and small-scale scattering models. In order to do that, the 3DZM must be validated as a technique that can recreate the results obtained through ultrasonic backscatter. At the current stage of development, the best way to pursue this goal is the development of more studies similar to the rabbit liver comparison study. With information gleaned from the previous experiment, another rabbit liver study, using healthy liver, will be completed. By reducing the errors of the previous trial, development of a quantitative link between 3DZM and QUS can begin.

In addition to a comparison study for liver, human fibroadenoma will also be used. The fibroadenoma tissue has a great deal of high level structure that varies a great deal spatially through the tissue. By comparing the 3DZM and QUS on a chemically fixed fibroadenoma sample, the effects of high level structure, such as anisotropy, can be examined in depth. The irregularity of fibroadenoma tissue also makes it an excellent candidate for testing a variety of scattering models. The simplicity of scattering models like the fluid-filled sphere will eventually give way to more complex models that better fit the underlying tissue structure. The computational domain of the 3DZM is a prime location to test such models.

A comparison study using a cell pellet is also of benefit. Using a cell pellet, a suspension

of a single cell type in a known background material, presents a nearly ideal case from the theoretical standpoint. Using a cell pellet allows for a very narrow distribution of cell sizes and shapes to be included in the study. Both ultrasonic backscatter measurements and 3DZMs can be constructed from the cell pellet. By examining such a simple media, strong statements about the relationship between 3DZM and QUS techniques can be made.

In addition to these comparison studies, the 3DZM must also become a more general tool for acoustics. Currently, there are plans to use 3DZMs to asses the denaturing of tissue due to the application of heat, and eventually for 3DZMs to be used in the study of high-intensity focused ultrasound (HIFU). HIFU is another application where the 3DZM's ability to generate both acoustic and structural information is extremely appealing.

8.3 Conclusion

3DZMs are a unique tool for the study of ultrasonic scattering in tissue. The ability to efficiently create 3DZMs from histology data was demonstrated, and the theory for analysis techniques and applications of the resulting 3DZMs were explored.

The impedance structure of microtissue, observable via the 3DZM method, is potentially a valuable tool in the further development of ultrasonic scattering models, QUS techniques, and other acoustics applications. Although the links between ESDs from 3DZMs and anatomical structures inside the volumes remains somewhat tenuous, further research into this method should prove to strengthen that bond.

QUS holds great diagnostic potential, and 3DZMs provide a powerful means to relate QUS results to actual tissue microstructure. That is, 3DZMs allow a connection to be made between QUS parameters and tissue pathology. This connection will be an essential step to propel QUS forward as an effective and noninvasive diagnostic imaging modality.

Appendix: ESD

ESD is an interpretation tool for the power spectrum of a 3DZM. The underlying physics of scattering in an inhomogeneous continuum are proportional to the Fourier transform of the spatial correlation function of the impedance distribution. By applying an FF model, the power spectrum can be viewed in relation to the power spectrum of discrete spherical scatterers. ESD, however, does not provide direct information on tissue microstructure. This work does not suggest that tissue is composed of a set of discrete spherical scatterers, whose sizes can be obtained through the 3DZM method. Very rarely will ESD have a one-to-one correlation with tissue structure. ESD is a way to process a power spectrum estimated from tissue into a more digestible form.

Despite not necessarily having a direct link to anatomic structures, ESD is still a valuable parameter. ESD is a commonly used QUS parameter, and has shown potential as a discriminant between tumor types [1, 3, 11].

The vast majority of problems with ESD estimation come from its simplicity and strict assumptions about the tissue microstructure. This is a major motivation for the use of 3DZMs. The 3DZM may provide a useful tool in the development of more complex scattering models, which give more direct information about anatomic structures. This link between acoustic scattering parameters and tissue microstructure is critical for the ultimate development of QUS as a clinically relevant tool.

References

[1] J. Mamou, "Ultrasonic characterization of three animal mammary tumors from three-dimensional acoustic tissue models," Ph.D. dissertation, University of Illinois at Urbana-Champaign, 2005.

[2] R. S. C. Cobbold, *Foundations of Biomedical Ultrasound*. New York, NY: Oxford University Press, 1997.

[3] M. L. Oelze, W. D. O'Brien, and J. F. Zachary, "Quantitative ultrasound assessment of breast cancer using a multiparameter approach," in *Proceedings of the 2007 IEEE Ultrasonics Symposium*, 2007, pp. 981–984.

[4] F. L. Lizzi, M. Astor, T. Liu, C. Deng, D. J. Coleman, and R. H. Silverman, "Ultrasonic spectrum analysis for tissue assays and therapy evaluation," *International Journal of Imaging Systems and Technology*, vol. 8, pp. 3–10, September 1996.

[5] F. L. Lizzi, M. Greenebaum, E. J. Feleppa, and M. Elbaum, "Theoretical framework for spectrum analysis in ultrasonic tissue characterization," *Journal of the Acoustical Society of America*, vol. 73, pp. 1366–1373, April 1983.

[6] M. F. Insana, R. F. Wagner, D. G. Brown, and T. J. Hall, "Describing small-scale structure in random media using pulse-echo ultrasound," *Journal of the Acoustical Society of America*, vol. 87, pp. 179–192, January 1990.

[7] J. Mamou, M. L. Oelze, W. D. O'Brien, and J. F. Zachary, "Identifying ultrasonic scattering sites from three-dimensional impedance maps," *Journal of the Acoustical Society of America*, vol. 117, pp. 413–423, January 2005.

[8] J. G. Proakis and D. G. Manolakis, *Digital Signal Processing*. Upper Saddle River, NJ: Pearson Prentice Hall, 2007.

[9] M. F. Insana and T. J. Hall, "Parametric ultrasound imaging from backscatter coefficient measurements: Image formation and interpretation," *Ultrasonic Imaging*, vol. 12, pp. 245–267, 1990.

[10] M. F. Insana and D. G. Brown, *Ultrasonic Scattering in Biological Tissues*. Boca Raton, FL: CRC Press, 1993, ch. Acoustic scattering theory applied to soft biological tissues, pp. 75–124.

[11] J. Mamou, M. L. Oelze, W. D. O'Brien, and J. F. Zachary, "Extended three dimensional impedance map methods for identifying ultrasonic scattering sites," *Journal of the Acoustical Society of America*, vol. 123, pp. 1195–1208, February 2008.

[12] P. Thevenaz and M. Unser, "A pyramid approach to subpixel registration based on intensity," *IEEE Transactions on Image Processing*, vol. 7, no. 1, pp. 27–41, 1998.

[13] M. F. Insana, T. J. Hall, and J. L. Fishback, "Identifying acoustic scattering sources in normal renal parenchyma from the anisotropy in acoustic properties," *Ultrasound in Medicine and Biology*, vol. 17, no. 6, pp. 613–626, 1991.